High resolution air quality simulation over Europe with the chemistry transport model CHIMERE

E. Terrenoire[(1)], B. Bessagnet[(1)], L. Rouïl[(1)], F. Tognet[(1)], G. Pirovano[(2)], L. Létinois[(1)], A. Colette[(1)], P. Thunis[(3)], M. Amann[(4)], L. Menut[(5)]

(1) INERIS –Parc Technologique Alata – BP 2 – 60550 Verneuil-en-Halatte – France
(2) RSE – Via Rubattino 54 – 20134 Milano – Italia
(3) JRC – Via Enrico Fermi 2749 – 21027 Ispra – Italia
(4) IIASA – Schlossplatz 1 – A-2361 Laxenburg – Austria
(5) Institut P.-S. Laplace, Laboratoire de Météorologie Dynamique, CNRS UMR 8539, Ecole Polytechnique, Palaiseau, France.

ABSTRACT

A high resolution air quality simulation (0.125°×0.0625° resolution) performed over Europe for the year 2009has been evaluated using both rural and urban background stations available over most of the domain. Using seasonal and yearly mean statistical indicators such as the correlation index, the fractional bias and the root mean squared error, we interpret objectively the performance of the simulation. Positive outcomes are: a very good reproduction of the daily variability at UB sites for O_3 (R=0.73) as well as for NO_2 (R=0.61); a very low bias calculated at UB stations for $PM_{2.5}$ (FB=-6.4%) and PM_{10} concentrations (FB=-20.1%). Conversely, main weaknesses in model performance include: the underestimation of the NO2 daily maxima at UB site (FB=-53.6); a slight overestimation of O_3 concentrations especially at UB sites, lower during summer than winter; an overall underestimation of PM_{10} and $PM_{2.5}$ concentrations, that is observed mainly over Eastern European countries (e.g. Poland); the overestimation of sulphates concentrations at spring time (FB=53.7%); finally, over the year, total nitrate and ammonia concentrations are better reproduced than nitrate and ammonium aerosol phase compounds. Obtained results suggest that, in order to improve the model performances, efforts should focus on the improvement of the emission inventory quality for Eastern Europeans countries and the urbanisation of CHIMERE to better account for the urban effect on meteorology and air pollutants concentrations.

Keywords

Air quality, model resolution, model performance evaluation, NO_2, O_3, PM_{10}, PM_{25}.

1. Introduction

Chemistry-Transport Models (CTMs) were initially designed to simulate ozone concentrations in the lower troposphere and a low horizontal resolution was sufficient to reach this objective. During the last decade, the air quality legislation has focussed more and more on particulate matter (PM) concentrations and CTMs had been equipped with aerosol modules. High PM concentrations are usually observed in urban areas (EEA, 2012) implying the increase of CTMs applications at urban scale.

The application field of CTMs is very large and includes: physico-chemical processes understanding (Bessagnet et al.(2010), Hodzic et al (2010), Jiménez-Guerrero (2011), Pirovano et al., 2012), assessment of emission control scenarios (Coll et al., 2010), past and future global air pollution trends (re)production (Colette et al. (2011)), chemical weather forecast (Balk et al. (2011), Kukkonen et al. (2011)), GEMS (http://www.gmes.info), GMES-MACC (http://www.gmes-promote.org) as well as natural hazard emergency response (Colette et al. (2011), Matthias et al. (2012)). Both constant evolution of model parameterisations and increased quality of input data, including meteorology and emissions, should foster frequent CTMs assessments. The evaluation process should be performed over comprehensive spatial and temporal data set in order to effectively quantify the model accuracy. A list of European model evaluation studies that took place during the last decade can be found in Pay

et al. (2011). The CHIMERE model itself has undergone several extensive evaluations (Vautard et al. (2007a); Van Loon et al. (2007)).

However, we note that CTMs are usually applied to wide domains at coarse resolution or at high resolution over small domains. The aim of the study is twofold: (i) have an accurate picture of air quality in Europe, and (ii) to comprehensively evaluate a fine resolution (0.0625x0.125°) CHIMERE simulation throughout the Europe using the largest set of monitoring stations available in 2009. In this study, the CHIMERE model has been improved in order to simulate the air quality at the urban scale.
The analysis is performed for ozone (O_3), nitrogen dioxide (NO_2), PM_{10} (Particles with an aerodynamic diameter < 10 µm), $PM_{2.5}$ (Particles with an aerodynamic diameter < 2.5 µm) and PM (Particulate Matter) compounds such as sulphate (SO_4^{2-}), nitrate (NO_3^-), total nitrate (HNO_3+ NO_3^-), ammonium (NH_4^+) and total ammonia (NH_3+NH_4^+).
Hence, the paper is organized as follow: section 2 is devoted to the description of CHIMERE, the methodology used to prepare the anthropogenic emissions and the set of observations used for the evaluation. Then, section 3 describes and analyses comprehensively the ability of the model to reproduce the different selected pollutants and finally, section 4 summarizes the main findings raised by the study and gives hints for further research related to high resolution regional modelling.

2. Tools and methodology

2.1 Model description

CHIMERE calculates the concentrations of the main chemical species that are involved in the physico-chemistry of the low troposphere. CHIMERE has been described in detail in several papers: Schmidt et al. (2001) for the dynamics and the gas phase module; Bessagnet et al. (2008, 2009) for the aerosol module; Vautard et al. (2005, 2007b) for the latest substantial model improvements. The aerosol model species are the Primary Particle Material (PPM), sulphates, nitrates, ammonium, secondary organic aerosols, sea-salts and dust. The particles size distribution ranges from 40 nm to 10 µm and the particles are distributed into 8 bins (0.039, 0.078, 0.156, 0.312, 0.625, 1.25, 2.5, 5, 10 µm). For more detail about latest developments one can refer to the online documentation (http://www.lmd.polytechnique.fr/chimere). For the study, we defined a nested fine resolution domain (328x416 grid boxes) that covers the whole Europe from 10.4375°W to 30.4375°E in longitude and 35.9062°N to 61.83375°N in latitude with a resolution of 0.125x0.0625° (Figure 7). Boundary conditions are based on monthly mean climatological profiles taken from the LMDz-INCA model for gaseous species (Hauglustaine et al. (2004)) and from the GOCART model for aerosols (Ginoux et al. (2001)). Data for comparison with observations are extracted from the lowest vertical level (20m). A complete and high resolution set of both biogenic and anthropogenic emissions are needed in order to perform CHIMERE computations. Six biogenic species (isoprene, α-pinene, β-pinene, limonene, ocimene, and NO) are calculated using the MEGAN model (Guenther et al. (2006)). We also account for wildfire emissions issued from the GFED3 (Kaiser et al. (2011)).

2.2 Meteorology

Meteorological data needed by CHIMERE were derived from ECMWF-IFS fields. The choice of feeding CHIMERE directly with ECMWF-IFS stems from the results of a sensitivity analysis performed comparing, for the studied are, the performance of WRF limited area model and the ECMWF-IFS (http://www.ecmwf.int/research/ifsdocs) against observed data. The analysis put in evidence a systematic overestimation of the wind speed by WRF, a feature confirmed also by other authors (Mass and Ovens. (2011); Jimenez and Dudhia. (2012)) As an example we draw the scatter plot of observed wind speeds (m/s) against IFS (red dots) and GFS/WRF (green dots) modeled values for European regional stations (Figure 1) and it clearly shows that WRF enhances the wind speeds by 25 % on average on the selected period (January 2009). Furthermore the direct use of ECMWF-IFS fields allows to avoid an ad-hoc meteorological Numerical Weather Calculation.

The IFS model has a 0.25° horizontal grid spacing (T799) from surface to 0.1 hPa (91 levels in total). It delivers typical meteorological variables (temperature, wind components, specific humidity, pressure, sensible and latent heat fluxes) that need to be vertically and horizontally interpolated on the CHIMERE grid (8 levels). Some additional variables are also diagnosed from the available fields, such as friction velocity and vertical wind speed, used to complete the description of vertical transport and turbulent diffusion.
However, the main limitation of such data is that the IFS regional scale data cannot represent correctly the urban scale meteorology observed in the urban canopy layer and the urban sub-layer. This is crucial as the urban canopy is affecting the wind circulation and the urban energy balance (Sarrat et al. (2006)) that will directly impact the transport and the vertical diffusion of primary pollutant over cities (e.g. O_3, NO_2 and PM). In order to integrate the influence of the urban canopy on meteorology, the wind speed and the vertical diffusion (Kz coefficient) are modified in the CHIMERE version used for this study. Usually, operational meteorological observations are performed outside urban areas (e.g. airport) for representativeness reasons. Some study reveals large differences between urban and rural winds (Fisher et al. (2005)) showing a wind speed ratio (rural/urban) up to a factor two. Another study shows that within the modeling case of Lisbon the ratio between wind speed inside the canopy and at the top of the urban sub-layer was within the range 0.1 to 0.6 (Solazzo et al. (2010)). For those reasons, we decided arbitrary to multiply the wind speed in the first CHIMERE layer by a factor 0.5 to limit the advection and diffusion of primary emitted pollutants.

In order, to estimate the potential impact of the wind and dispersion coefficient (Kz) urban correction, we performed a sensitivity test over January 2009. Figure 2 shows the difference in concentration between the simulation using the urban correction and the simulation which is not using any correction over urban areas for four main pollutants: NO_2, O_3, PM_{10} and $PM_{2.5}$. For all examined pollutants, we note a rather strong impact over all major European cities. For NO_2, we observe an increase in concentrations ranging from a few ppb (suburban areas) to 12-15 ppb (e.g. Paris, London, Madrid and Milan). Consecutively to the NO_2 concentrations increase over cities, we note a decrease of O_3 (NO_2 titration essentially), not only over the main cities (5 ppb on average up to 7 ppb in the city centre), but also over medium size cities (1 to 2 ppb). However the strongest impact is observed for the PM_{10} and $PM_{2.5}$ and especially for PM_{10} where an increase from a few to 40 $\mu g/m^3$ for cities such as Milan or Paris is seen but up to 70 $\mu g/m^3$ for the region of Katowice in south Poland.

2.3 Anthropogenic emissions

The anthropogenic emission pre-processor transforms raw yearly anthropogenic emissions (ton/year/cells) into a CHIMERE compliant spatialised emission dataset. The raw emission data of the main air pollutants (Non Methanic Volatile Organic Compound (NMVOC), NOx, CO, SO_2, NH_3, PPM) comes from the annual inventory that is delivered by the European Monitoring and Evaluation Program (EMEP) (Vestreng (2003)). Emissions are provided per activity sector, according to the level 1 of SNAP sectors classification:

1. Combustion in energy and transformation industries
2. Non-industrial combustion plants
3. Combustion in manufacturing industry
4. Production processes
5. Extraction and distribution of fossil fuels and geothermal energy
6. Solvent and other product use
7 Road transport
8. Other mobile sources and machinery
9. Waste treatment and disposal
10. Agriculture
11. Other sources and sinks

Figure 3 displays the five main steps that can be identified in the anthropogenic emission pre-processing (1) the spatial regridding of the raw emission to comply with the CHIMERE grid, (2) the

temporal disaggregation, (3) the chemical speciation, (4) the hourly disaggregation and (5) the surface flux calculation within CHIMERE.

2.3.1 Spatial reggriding and vertical allocation of anthropogenic emissions

The first step of emission processing consists in regridding the EMEP anthropogenic emission inventory available over a 0.5°x0.5° resolution grid onto the CHIMERE computational grid using a set of suitable proxy variables. We derived most of these variables from the USGS Land Uses database, whose high resolution (1km) preserves accuracy on emission spatialisation. Twenty height landuse categories exist in the USGS database but only "crops", "grasslands", "urbanized area" and "forest" categories are used to downscale the emissions.
For this study, the emission pre-processor has been modified to allow emissions from SNAP2 to be disaggregated according to the population density. The goal of this approach is to better capture the spatial variability of the SNAP2 emissions sector. The population data were provided by the Joint Research Centre (JRC) over a regular grid at 0.083x0.083° horizontal resolution. For the elaboration of the SNAP2 emissions, we also made a distinction between gaseous and PPM species to better reallocate the anthropogenic biomass burning emissions (SNAP 2) over the rural areas. Indeed, according to the French national spatialised emission inventory, available at municipality level and derived using the bottom-up approach (MEDDTL, Ministère de l'Ecologie et du Développement Durable, 2004), there is clear evidence that $PPM_{2.5}$ emissions per inhabitant sharply decrease when the population density increases (Figure 4). This is due to the increase of the relative contribution of wood burning in the fuel mixture moving from urban centres to rural areas (e.g. due to increase in domestic fireplaces). This effect is noticeable only for PPM2.5, because biomass burning emissions are less influent on gas phase pollutant than particulate matter.

Finally, total emissions used in CHIMERE are computed by simply averaging the emission fluxes of each landuse/population cell belonging to the same "mother" CHIMERE cell.

As an illustration, Figure 5 shows the spatial distribution of the $PPM_{2.5}$ emissions from the SNAP2 sector derived from the EMEP emission inventory. The picture shows the total annual primary particle emission <2.5µm obtained using the pre-described modifications. Compared to the original method, we observed that around the medium and great size cities SNAP2 emissions using the population proxy are increased. This is due to the fact that when using the landuse proxy, emissions from each kind of Land Use (LU) cells have the same weight, thus giving rise to a flatter distribution than using population. Considering for example an EMEP cell including a big city as well as a small town, following the LU approach, emissions are modulated in the same way over urban cells of both areas, whereas using population, most of the emissions are allocated just in the big city.

The vertical reparation of the emission into the different levels of the CTM is known to be of great importance (Bieser et al. (2011)). It is calculated according to the SNAP sector for each primary pollutant of the inventory following the calculation of Bieser et al. (2011) (Table 1). We also add a new layer (0-40m) compared to the original EMEP setting. Note that for S2, S6, S7, S8 and S10 all the emissions are released into the first level of the model.

2.3.2 Chemical speciation

Annual NOx emissions were speciated into NO, NO_2 and HNO_2 using the coefficients recommended by IIASA (personal communication, Table 2). For NMVOC, a speciation was performed over 32 NMVOC NAPAP classes (Middleton et al. (1990)). In a second time, an aggregation step is performed for the lumping of NMVOCs into model species following Middleton et al. (1990). Time disaggregation was done on the basis of GENEMIS data using monthly, weekly and hourly coefficients depending on the activity sector (Society et al. (1994)). Finally, hourly values of surface anthropogenic emissions are available for PPM and 15 primary gaseous pollutants: NO, NO_2, CO, SO_2, CH_4, and the ten following non-methane volatile organic compounds (NMVOC): Ethane, n-

butane, ethene, propene, o-xylene, formaldehyde, acetaldehyde, methyl, ethyl-ketone, ethanol and ethanol.

2.3.3 SNAP 2 emission temporal modulation

For SNAP 2, we also propose a new temporal profile derived according to the daily "degree day" (degdays) concept. The degree day is an indicator used as a proxy variable to express the daily energy demand for heating. The degree day for a day "*j*" is defined as: $D_j = max(0, 20\text{-}T_D)$ where T_D is the daily mean 2m temperature. Therefore, a first guess daily modulation factor could be defined as: $F_d = D_j/\overline{D}$ with $\overline{D}$ the annual averaged "degree day". Considering that SNAP 2 emissions are not only related to the air temperature (e.g. emissions due to production of hot tap water), a second term is introduced in the formula by means of a constant offset C. To better assess the influence of this offset, C can be expressed as a fraction of $\overline{D}$ (degree day annual average). Considering:

$$C = A.\overline{D} \text{ where } A = 0.1 \text{ (defined by user),}$$

the daily modulation factor (F_j) is therefore defined as:

$$F_j = D'_j/\overline{D}' \text{ where } D'_j = D_j + A\,.\overline{D} \text{ and } \overline{D}' = (1 + A).\overline{D}$$

Note that F is mass conservative over the year and replaces the original monthly and daily modulation factors.

As an illustration, Figure 6 shows the 2009 daily modulation factor applied to the SNAP 2 emissions at three different locations both geographically and climatically: Katowice (Poland), Paris (France) and Madrid (Spain). We observe that the highest factors for the three locations are logically seen during the winter period and the lowest ones during the summer. This means, for example, that during the cold periods the emission from SNAP 2 can be up to three times more intense (e.g. beginning of January for Madrid or end of February for Paris) than during the spring or the autumn periods. Interestingly, we note that in Katowice during the beginning of the year the factors are relatively lower than at the two other locations meaning that over this period the different between the daily mean temperature and the annual mean is lower in Katowice than the one at the two other locations. In other word, Madrid and Paris experienced a cold period in January and at the end of February, respectively, whose the intensity was higher than in Katowice. Inversely, at the end of the year, all the locations experienced a cold outbreak of the same intensity relatively to their local annual mean temperature.

2.4 Observation data

Observed data come from two different databases. The first one is Airbase (http://acm.eionet.europa.eu/databases) gathering regulatory data reported by Member States according to the air quality. The second one is related to the EMEP network (http://www.emep.int/). Only stations below 750 m in altitude with 75% over the year are selected. Figure 7 displays the spatial distribution of the AIRBASE (green for Rural Background (RB) and blue for Urban Background (UB)) and the EMEP stations (red) used for the evaluation. The stations spatial repartition is homogenous over the populated regions of Western Europe, while several gaps are noted in Eastern European and for Balkans countries. Table 3 shows that a high number of stations is available for most of the pollutants in which we are interested in (NO_2, O_3 and PM_{10}). Differently fewer stations are available for $PM_{2.5}$ both at UB sites (267) and especially at RB sites (92). The EMEP database includes less sites than Airbase, but it is the only European network providing PM speciation data, that are crucial to investigate in deeper detail the model performance. Details about the station type classifications and the different measurements techniques are available through the previously quoted Airbase and EMEP websites.

In this paper, we perform an "operational evaluation" (Dennis et al. 2010). The evaluation is based on the comparison of observation and modelled values using statistical indicators and graphic methods. We have selected different statistical indicators for their ability to diagnose the model performance

from different perspective including temporal correlation, bias, absolute error, agreement between observation and modelled values. Therefore, along with the observed (OM) and modelled (MM) meanconcentration, we calculate: the observed (σ_obs) and modelled (σ_mod) standard deviation, the correlation index (R), the root mean square error (RMSE), the fractional bias (FB), the fractional error (FE) and the index of agreement (IA). Details about the calculation of the statistics, performed using the Atmospheric Model Evaluation Tool software (AMET) can be found in Appel et al. (2011) and in the **APPENDIX *A***. The performance evaluation is based on yearly and seasonal statistics using the daily values of all stations available for the given typology (UB and RB).

3. Model results

Table 4 and Table 5 display the yearly and seasonal statistical scores for NO_2, O_3, PM_{10}, and $PM_{2.5}$ at RB and UB Airbase stations, respectively. Table 6 displays the same metrics computed at EMEP sites, thus including also sulphate (SO_4^{2-}), nitrate (NO_3^-), total nitrate (HNO_3+ NO_3^-), ammonium (NH_4^+) and total ammonia (NH_3+NH_4^+). Figure 8 and Figure 9 show the daily box-whisker plots time series of NO_2, O_3, PM_{10} and $PM_{2.5}$ computed at RB and UB stations respectively. Figure 10 shows the box-whisker plots time series for sulphate (SO_4^{2-}), total nitrate (HNO_3+ NO_3^-), total ammonia (NH_3+NH_4^+) calculated at EMEP stations.

3.1 Nitrogen dioxide

Figure 9 and Figure 10 show that along the year, CHIMERE catches nicely the temporal variability of NO_2 both at RB (R=0.68) and UB (R=0.61) sites. At UB stations, it underestimates significantly the concentrations over the year (FB=-53.6%) and especially during the winter season (FB=-63.9). This behaviour is also observed at RB sites with however a lower bias (FB=-46.5% in winter) than UB sites. The calculation of the quantiles allow to conclude that at RB sites, the lowest values are the best reproduced while at UB sites the maxima are slightly better caught by the model than the minima. For UB sites, the dissatisfied performance can be explained by the general tendency to underestimate NOx urban emissions (e.g. Eastern European cities) whose impact is magnified by the winter stagnant conditions that increase the NO_2 observed concentrations at ground level (e.g. 5-20 January). Further investigation of the model behaviour over urban areas performed using the DELTA tool (Thunis et al., 2012), pointed out that the performance was significantly higher over the main European cities (e.g. capitals) UB stations than over the UB stations of medium and small cities. Figure 11 shows the scatter plot of the modelled versus then observed NO_2 concentrations ($\mu g/m^3$) at the UB stations (*N*=105) of 30 major cities across Europe. The blue dot represents the mean of the 105 UB stations. We note that the use of those selected stations reduces significantly the bias between observed and modelled concentrations from 4.58 ppb when using all UB available stations to 1.31 ppb when using only major cities UB stations (factor 3.5). This indicates that the urban correction is not sufficient to correctly capture the NO_2 concentrations which are underestimated over small cities. At this point of the study, the reasons for this underestimation remain unclear and could be due to the horizontal resolution not enough fine to correctly simulate the urban meteorology on small cities as well as the spatial gradient of the emissions.

Nevertheless, at RB sites the interpretation of the negative bias is more difficult to explain. A possible explanation could be inferred noting that CHIMERE usually performs better in reproducing the temporal variability of the observed concentrations (e.g. standard deviation and correlation index) than the mean values. This result seems to indicate a lack in the oxidised nitrogen burden, due to an underestimation of the NOX emissions.

3.2 Ozone

Overall, daily temporal variability of O_3 concentrations is very well simulated both at rural (*r*=0.77) and UB sites (R=0.73). The comparison of the quantiles of the modelled and observed concentrations (Figure 8 and Figure 9 respectively) show that the highest values are well reproduced at both RB and UB stations, while lower quantiles are overestimated. Indeed, the modelled values show a systematic positive bias which is higher at UB (FB=25.2%) than at RB sites (20.1%). At urban sites, this tendency can be related to the lack of titration by NO_2 of the O_3 due to the previously described underestimation of NO_2 especially during the winter. The bias has a seasonal variation with low

positive FB that is observed at UB sites in the summer (14.9%) and a high one during the winter (35.6%). Similar tendency is seen at RB sites but with a lower magnitude. The RMSE indicator also confirms the fact that at UB sites during the winter the model has a tendency to overshoot the maxima. However, at RB sites, the RMSE stays rather constant over the entire year (8.5 ppb in mean). The tendency is likely to be related to the overestimation of the background concentrations by CHIMERE previously described in Chen et al., 2003 and Szopa, 2009.

3.3 PM_{10} and $PM_{2.5}$

At UB stations, R gets its highest value during the autumn (0.56) and its lowest value during the summer and the winter (0.47). Conversely, the FB is lower during the warm season (-12.2% at spring time) than in winter (-36.6%). At RB site, over the year, the model agrees better in terms of correlation compared to the UB sites (0.62 against 0.52 at UB sites), especially during winter (0.67 against 0.47 at UB stations) than summer (0.50 against 0.47 at UB sites). It is worth noting that the RMSE is increasing by a factor two on average in the winter compared to the other seasons during which it stays rather constant (e.g. 34.8 µg/m^3 during winter and 17.33 µg/m^3 in spring at UB sites).
The behaviour of $PM_{2.5}$ is comparable to PM_{10} in terms of statistical indicators. However, we note for $PM_{2.5}$ a yearly R value higher than PM10 at both UB (0.65) and RB sites (0.71) indicating that, on a yearly basis, CHIMERE reproduces better the temporal variability across Europe of $PM_{2.5}$ than PM_{10}. At UB sites, CHIMERE performs better in autumn (0.69) than in summer (0.46). The highest correlation index is observed at RB sites during the winter (0.74). The FB is very low during the autumn at UB stations (-4%) but higher during the winter (-24.6%). We underline that CHIMERE gives in terms of bias, over the year, a good performance concerning the $PM_{2.5}$ concentrations at UB stations (FB=-6.4%). At RB sites the FB is always positive except during the winter (-8.7%) and the maximum is observed during the autumn (14.2%) and the minimum during the summer (0.4%). Note that the overestimation of $PM_{2.5}$ at RB sites, as shown by the low quantile of the modelled concentrations is limited to the lowest values. In both cases, CHIMERE performed better in reproducing the low PM_{10} and $PM_{2.5}$ concentrations as shown by the quantiles.

PM_{10}, $PM_{2.5}$ and PM speciation data are available on several EMEP sites. As previously observed at the Airbase RB stations, CHIMERE overestimates the $PM_{2.5}$ concentrations at the EMEP RB stations (Table 6). By opposition to the Airbase RB stations, the PM_{10} are overestimated at EMEP stations (FB=2.9%). A strong inter-seasonal variability is observed with the lowest FB noted during the summer for PM_{10} (-2.3%) and $PM_{2.5}$ (5.8%) and the highest during the winter for PM_{10} (-14.4%) and during the autumn for $PM_{2.5}$ (15.7%). As observed by the Airbase station, the highest correlation coefficient is found during the winter for both PM_{10} (0.68) and $PM_{2.5}$ (0.77). Similarly, the highest RMSE error is found during the winter for PM_{10} (12.3 ppb) and $PM_{2.5}$ (10.7 ppb). As the model performance for PM_{10} is reflected by the quality of the reproduction of its different components, we look at the capacity of the model to reproduce three main PM compounds: sulphate, nitrate and ammonium species.

3.4 Sulphate

Sulphuric acid is produced from the oxidation of sulphur oxides, which in turn form sulphate particle. Secondary sulphate aerosol occurs predominantly in the accumulation mode; diameter between 0.1 and 1.0 µm (Altshuller, 1982). Both oxidants and SO_2 availability are the limiting factors for sulphate formation. In 2009, the 37 stations available over Europe indicate that the highest concentrations are measured during winter and spring (Figure 10 and Table 6). This tendency is reproduced by the model (R=0.57 during spring and 0.52 during the winter) but some maxima are overestimated especially during spring. Consequently, the FB is rather low during the summer (FB=20.1%) but indicates a strong overestimation during spring time (FB=53.7%). This tendency is in opposition with the one calculated by CALIOPE (Pay et al., 2012) and CMAQ (Matthias et al. 2008). Conversely to

CHIMERE, CALIOPE and CMAQ tend to underestimate the sulphate surface concentrations over Europe along the year.

If we look at the seasonal trend, the one simulated by CHIMERE over Europe is in agreement with the study of Baker and Scheff, 2007 in north America but it is in opposition with what is observed over Spain using CMAQ model (Pay et al. (2011)). In this case, the highest sulphate concentrations are noted in the summer due to high oxidation of SO_2 during this period. Some missing processes concerning the dry deposition of SO_2 could be the main reason that explains the general overestimation of sulphate by CHIMERE (Baker and Scheff, 2007).

3.5 Particulate nitrate and total nitrate

Nitrogen dioxide (NO_2) and nitric acid (HNO_3) are the two main gas precursors than can react together to form ammonium nitrate (NH_4NO_3) depending on the temperature and the relative humidity (RH) (Ansari and Pandis, 1998). Nitric acid can be produced through either homogeneous reaction of NO_2 with OH radical (daytime), reaction of NO_3 with aldehydes or hydrocarbons (daytime) or hydrolysis of N_2O_5 in the troposphere (night time) (Richards, 1983; Russell et al. 1986). Note that during cold temperatures, the equilibrium of the NH_4NO_3 system shifts toward aerosol phase. At low RH, ammonium nitrate is solid but if RH overcomes the deliquescence threshold it turns to aqueous phase ($NH_4^+ + NO3^-$) (Bauer et al. 2011).

Sulphuric acid plays a crucial role in the formation of nitrate and ammonium. Sulphate tends preferentially to react with ammonia to form $(NH_4)_2SO_4$. Two regimes can be identified: the ammonia poor and the ammonia rich regime (Bauer et al. 2011). In the first case, there is not enough NH_3 to neutralize the available sulphate. In the second case, sufficient ammonia is present to neutralize the sulphate and the remaining ammonia is available to react with nitrate to produce NH_4NO_3 which will be in aqueous phase to form nitrate and ammonium if meteorological conditions are favourable.

Using the 17 EMEP stations, we show that the nitrates are strongly underestimated along the year (FB= -103.5%) but rather high R value is noted during the winter (0.67) indicating the good reproduction of the temporal variability of nitrate concentrations by CHIMERE during this period (Table 6). The lowest FB is observed during the winter (-68.4%). Winter is also linked to the highest measured and modelled nitrate concentrations. During cold periods, the formation of NH_4NO_3 is favoured and the associated low dispersive conditions enhance the increase of nitrate during these periods. Different explanations concerning the general underestimation of nitrate can be considered. First, where ammonia limits the formation of nitrate, the underestimation could be explained by the previously described overestimation of sulphate. Secondly, the coarse nitrate chemistry is not represented in CHIMERE in the operational version leading to an underestimation of the coarse mode nitrate aerosol. This process was implemented in a research project in CHIMERE (Hodzic et al., 2006). Typical reactions involved in the coarse nitrate chemistry include the neutralisation of acidic aerosol particle (NO_3^-) by different basic positive ions such as Ca^{2+} and Mg^{2+}. Na^+ and Cl^- are also involved along coastal areas where high sea salt (NaCl) concentrations are observed. Differently, the total nitrate concentrations (Figure 10) is much better reproduced than the nitrate alone (r=0.66 during the winter) except during the summer (0.16). The order of magnitude of the FB indicates an underestimation by a factor 2 over the year.

3.6 Particulate ammonium and total ammonia

Along with sulphate, ammonium appears to be the best SIA compound reproduced by CHIMERE (Table 6). The FB is rather low (27.1% over the year) and shows the lowest overestimation during the summer (7.5%). Associated to a good correlation index (0.77), winter is the season during which CHIMERE reproduces the best the observations. A similar tendency is also noted when using the CMAQ model over Spain and the U.K (Pay et al. 2012; Chemel et al. 2010).

Similarly, the total ammonia (Figure 10) is nicely reproduced by CHIMERE with a very low bias observed during the winter (FB=-1.8%). The performance is decreasing during the summer where the model is underestimating the most the observations (FB=-10.7%). As ammonium is overestimated most of the year, the underestimation of total ammonia would lead to the fact that ammonia concentrations are underestimated except during spring and autumn. Recent work concerning the

improvement of the magnitude, the temporal variability and spatial distribution of NH_3 emissions from the agricultural sector had been done for France (Hamaoui-Laguel et al. 2012). Unfortunately, a robust monthly time-profile for the NH_3 emission from fertilizer is yet to be finalized for Europe (Menut and Bessagnet, 2010) before its implementation in the model.

3.7 Spatio-temporal variability of the modelled concentration fields

In this section, we analyse the 2D annual mean concentrations maps of NO_2, O_3, PM_{10} and $PM_{2.5}$ (Figure 12). On each map, the observed values for each station are represented by a coloured dot. We also draw the winter (December-January-February) and the summer (June-July-August) seasonal means to analyse the inter-seasonal variability of the modelled concentrations for NO_2 and O_3 (Figure 13), PM_{10} and $PM_{2.5}$ (Figure 14) and the SIA species (Figure 15 and Figure 16). For NO_2, O_3, $PM_{2.5}$ and PM_{10}, we include the observed concentrations (dots) for both types of stations (RB and UB).

For NO_2, the concentrations are directly linked to the emissions mainly from SNAP 2 (non-industrial combustion plants), 7 (road traffic) and 8 (other mobile source). Therefore, as expected, Figure 12 shows that the highest annual mean concentrations are located over urban area and along ship tracks (Atlantic, Channel, and Mediterranean Sea). We identify specific areas with high concentrations: the Pô-Valley, Paris, Benelux, London, south of Poland (e.g. Katowice), Athens, Madrid and Barcelona. For those specific areas and generally over Europe the concentrations are much higher during the winter and than during the summer due to higher emissions and low vertical dispersion (e.g. shallow boundary layer height, low dispersion conditions, thermal inversion). Ship tracks in the Mediterranean Sea, the coast of Portugal and especially the Channel are characterised by rather high NO_2 annual modelled concentrations between 2 and 12 ppb. The observation values represented by the dots show overall a slight underestimation of the NO_2 concentrations. However two main areas located over the south of Poland (Katowice) and some parts of Romania (industrial hot spots) show a stronger underestimation (10-20 ppb). We also note some areas where the observations are overestimated: Paris, London, Madrid, Barcelona and Athens. For those areas, the methodology used to downscale the national annual emission could be the reasons of such a feature.

Generally we note that CHIMERE slightly overestimates the O_3 concentrations over Europe. Figure 12 shows that the highest annual mean concentrations are located below the 45° line of latitude where the strongest photolysis over Europe occurs (from 30 ppb over the coasts to 48 ppb over the sea). The maximum of O_3 is modelled during the summer while the winter seasonal mean is bellow 30 ppb over most of Europe reaching near zero values in the Benelux, the Pô Valley, Germany and Poland. The highest summer concentrations are calculated over and around the Mediterranean Sea where low boundary layer height compared to continental PBL height and strong photolysis are favourable conditions to high ozone concentrations (up to 56 ppb). Note that during the warm period most of the capitals across Europe are characterised by ozone decrements due to the ozone titration by NOx in those urbanised areas.

For PM_{10}, the overall picture shows that the highest concentrations (from 20 to 30 $\mu g/m^3$) are located at the south of a line which goes from the south of Portugal to the north of Poland (Figure 12). The annual mean concentrations are nicely modelled (slight underestimation) over the continent except over cities such as Milan, Paris and Krakow where CHIMERE overestimates the observations. In winter, the calculated concentrations are maximal over the continent (between 10 and 30 $\mu g/m^3$) with lower concentrations over central Spain (10 $\mu g/m^3$). Hot spots are located over the main European cities and over industrial primary emissions areas (e.g. Romania and Bulgaria). In summer, the concentrations are strongly influenced by the dust level at the boundary condition in the south part of the domain (up to 40 $\mu g/m^3$) and the city signal is really low except for Katowice, Milan and Paris (up to 40 $\mu g/m^3$). Over the continent the concentrations are lower by a factor of two. In winter, much lower concentrations are modelled over the Mediterranean Sea (16-18 $\mu g/m^3$) where the influence of dust at the boundary condition is the lowest. Primary emissions from the main cities and industrial areas have its strongest intensity. Three hot spots can be identified: the Po valley, the south of Poland

(Katowice region) and the south of Romania (area of Bucharest). Indeed, very high PM_{10} concentrations are modelled all over the year over those areas. The strong primary emissions (both SNAP 2 and 7) are the main reasons for this critical situation as well as favourable meteorological conditions for SIA formation (low vertical and horizontal dispersion, high level of humidity during the cold seasons) that play also a major role in the build up of high PM_{10} concentrations especially in the Pô valley.

For $PM_{2.5}$ (Figure 12), the pattern is similar to the one described for PM_{10} (Figure 14). The highest concentrations are calculated all along the year over the Pô valley (30 to 60 $\mu g/m^3$) except in summer (16 to 20 $\mu g/m^3$). Note that, at spring, high concentrations are calculated over the east of the Mediterranean Sea and are partially linked to the production of sulphate in the fine aerosol mode. The observations show a good agreement with the modelled concentrations fields but a general underestimation is clearly identified over some Eastern Europe countries such as Poland and Bulgaria.

For sulphate (Figure 15), during the winter, a sharp zonal gradient is observed with minima observed in Western Europe (2 $\mu g/m^3$ on average) and the maxima on Eastern Europe (up to 8 $\mu g/m^3$). The highest concentrations are located near the main SO_2 emission areas which correspond to the industrial area in Romania, Bulgaria, Bosnia, Serbia, Hungary and south Poland that used sulphur-rich coal (e.g. in the Katowice region). In summer, the gradient is meridional with a maximum in the south of the domain along the coast of northern Africa. In summer, sulphate results from the gas oxidation of SO_2, it is mainly produced in the Mediterranean Sea where emissions from ships are high and intense photolysis allows the production of oxidant radicals (e.g. OH radical).

For ammonium and nitrate (Figure 16) a strong seasonal variability is modelled with a low modelled concentrations observed in the summer and high one during the winter. Nitrate is less influenced by its emissions precursors compared to sulphate. However, we note that highest modelled concentrations are seen during the winter over the Pô valley (up to 15 $\mu g/m^3$), over the Benelux (6 $\mu g/m^3$) and the south of Germany (8 $\mu g/m^3$). High ammonium concentrations are also modelled over the Pô valley (up to 5.2 $\mu g/^3$) and other countries such as the Benelux, south of Germany, Poland, Hungary and the south of Romania where concentrations can reach 3 $\mu g/m^3$.

4. CONCLUSIONS

A high resolution simulation of air quality with CHIMERE (0.125°×0.0625°) over most of Europe has been evaluated using both at rural and urban background stations for the year 2009. In this CHIMERE version, the main updates and model developments include:

- The use of the population density proxy to downscale the SNAP2 emissions,
- The update of the emission layers depths and vertical emission injection heights,
- A new NOx speciation,
- The modulation of the SNAP2 emission according the 2 m air temperature,
- The urban correction of Kz and wind speed variables.

First, different seasonal and yearly mean statistical indicators have been calculated to interpret objectively the performances of the CHIMERE model. Positive outcomes are:

- A very good reproduction of the NO_2 day to day variability at UB sites (R=0.61) and especially O_3 (R=0.73).
- A good reproduction of the $PM_{2.5}$ day to day variability both at RB (R =0.71) and UB (R =0.65) stations
- A very good performance concerning the reproduction of PM_{10} concentrations (FB=-5.5%) and for $PM_{2.5}$ concentrations (FB=-6.4) at UB stations on an annual basis.

- For sulphates, the model performs rather well during the summer (FB=20.1%)
- The total nitrate concentrations variability is much better reproduced than nitrate stand-alone with a high R over the year (R >0.56).
- Finally, the total ammonia is better reproduced during winter (FB=-1.8%) than the other seasons.

However, difficulties concerning the model performances have been identified:

- An underestimation of the daily maxima for NO_2 especially at UB sites (FB=-53.6%),
- A systematic but rather low overestimation of O_3 concentrations lower during the summer than during the winter especially at UB sites,
- An underestimation of $PM_{2.5}$ concentrations over Eastern European countries (e.g. Poland and Bulgaria),
- An overestimation of the sulphate concentrations at spring (FB=53.7%),
- An underestimation of total nitrate by a factor 2 over the year mainly caused by the strong summer underestimation due to the missing coarse nitrate formation in CHIMERE.

Therefore, three main areas of work in order to improve the CHIMERE performance have been identified:

- The urbanisation of CHIMERE to account for the urban effect on meteorology and therefore on both the primary and secondary air pollutants concentrations,
- The introduction of the coarse nitrate chemistry and a advanced parameterisation accounting for the wind-blow dust emissions,
- The introduction of existing national bottom-up approach emission databases (e.g. France, Spain) into the existing European emission inventory (e.g. MACC) for major cities and eastern European countries.

Acknowledgements :

This study was partly funded by the French Ministry in charge of Environment. This work was done under the auspices of the European project EC4MACS (EU LIFE, www.ec4macs.eu).

565

566 *Table 1: Vertical emissions profiles (%) for each SNAP (S) sector*

Injection height (m)	20	92	184	324	522	781	1106
S1	0	0	0.25	51	45.3	3.25	0.2
S2	100	0	0	0	0	0	0
S3	6	16	75	3	0	0	0
S4	5	15	70	10	0	0	0
S5	2	8	60	30	0	0	0
S6	100	0	0	0	0	0	0
S7	100	0	0	0	0	0	0
S8	100	0	0	0	0	0	0
S9	0	0	41	57	2	0	0
S10	100	0	0	0	0	0	0
S11	100	0	0	0	0	0	0

567

568 *Table 2: NOx speciation used in CHIMERE for the simulation*

	S1	S2	S3	S4	S5	S6	S7	S8	S9	S11
NO	95.0	95.0	95.0	95.0	95.0	95.0	83.5	90.0	95.0	95.0
NO2	4.5	4.5	4.5	4.5	4.5	4.5	15.0	9.2	4.5	4.5
HNO2	0.5	0.5	0.5	0.5	0.5	0.5	1.5	0.8	0.5	0.5

569

570 *Table 3: Number of stations available per species and network over the domain of simulation*

	NUMBER OF STATIONS		UNIT
	UB	RB	
AIRBASE			
NO_2	770	300	ppb
O_3	586	361	ppb
PM10	677	238	$\mu g/m^3$
PM2.5	267	92	$\mu g/m^3$
EMEP			
NO_2	X	24	ppb
PM10	X	21	$\mu g/m^3$
PM2.5	X	17	$\mu g/m^3$
SO_4^{2-}	X	37	$\mu gSg/m^3$
NO_3^-	X	17	$\mu gN/m^3$
TNO_3	X	26	$\mu gN/m^3$
NH_4^+	X	17	$\mu gN/m^3$
TNH_3	X	14	$\mu gN/m^3$

571

572

Table 4: Annual and seasonal scores calculated using the whole RB Airbase set of stations. The statistics are: the Observed Mean (OM), the Modelled Mean (MM), the standard deviation of the observations (σ_obs) and modelled values (σ_mod), the correlation index (R), the Root Mean Squared Error (RMSE), the Fractional Bias (FB in %) and the Fractional Error (FE in %) and the Index of Agreement (IA). N_{OBS} is the number of observations. Units for each pollutant are reported in Table 3, R and IA are unit less. A description of statistics is given in Appendix A.

	N_{OBS}	OM	MM	σ_obs	σ_mod	R	RMSE	FB	FE	IA
NO2										
Annual	98833	6.55	4.63	5.75	4.37	0.68	4.67	-33.90	53.40	0.77
Spring	25173	5.66	3.94	4.41	3.50	0.63	3.90	-37.90	56.10	0.74
Summer	24168	4.22	3.27	3.15	2.60	0.53	2.97	-26.00	50.40	0.70
Automn	24929	6.58	5.04	4.97	4.56	0.67	4.20	-29.50	50.40	0.79
Winter	16105	10.23	6.22	8.36	5.59	0.69	7.26	-46.50	59.30	0.74
O3										
Annual	122518	28.60	33.45	11.13	8.65	0.77	8.59	20.10	26.30	0.81
Spring	31787	35.12	38.71	9.19	6.35	0.59	8.29	11.90	19.40	0.71
Summer	31865	33.91	37.77	9.30	6.28	0.65	8.05	13.10	19.50	0.73
Automn	30074	23.50	30.26	9.74	7.12	0.71	9.64	30.60	34.90	0.72
Winter	18941	21.65	27.56	8.68	8.08	0.70	8.82	27.40	33.10	0.75
PM10										
Annual	77828	20.67	17.90	14.93	9.65	0.62	12.02	-5.50	37.70	0.73
Spring	19656	21.41	20.01	14.25	9.54	0.60	11.49	2.10	36.00	0.73
Summer	19639	17.17	14.41	8.63	6.54	0.50	8.26	-13.30	35.70	0.68
Automn	19459	19.28	18.19	12.36	10.16	0.64	9.77	0.30	37.30	0.79
Winter	12374	27.20	18.94	22.45	11.11	0.67	18.95	-20.30	43.60	0.68
PM25										
Annual	27574	13.69	12.78	12.59	7.96	0.71	8.99	7.50	40.40	0.79
Spring	6737	14.80	14.71	12.05	7.44	0.67	8.95	13.20	39.10	0.76
Summer	7043	9.87	9.11	5.50	3.74	0.53	4.80	0.40	36.90	0.69
Automn	7151	12.29	12.44	10.29	7.68	0.71	7.31	14.20	42.10	0.81
Winter	4186	20.05	15.16	19.78	10.70	0.74	14.73	-8.70	43.50	0.75

Table 5: Annual and seasonal scores calculated using the whole UB Airbase set of stations. The scores and the associated units are identical to the ones available on Table 4.

	nb_dly_obs	OM	MM	σ_obs	σ_mod	R	RMSE	FB	FE	IA
NO_2										
Annual	264005	13.15	8.57	8.14	8.09	0.61	8.48	-53.60	66.60	0.73
Spring	67205	12.34	7.91	6.93	7.71	0.59	8.02	-57.80	70.40	0.71
Summer	65960	8.97	6.64	5.14	6.53	0.51	6.34	-44.00	63.70	0.68
Autumn	65665	13.39	9.13	7.52	8.40	0.64	8.05	-51.70	64.00	0.74
Winter	42984	18.65	10.77	9.98	9.15	0.64	11.37	-63.90	70.50	0.70
O_3										
Annual	190716	24.90	30.71	10.95	9.43	0.73	9.62	25.20	33.40	0.79
Spring	51219	30.31	35.30	9.21	7.91	0.56	9.54	16.90	25.90	0.69
Summer	51195	31.08	35.29	9.36	7.28	0.62	8.60	14.90	22.70	0.73
Autumn	46215	19.80	27.46	9.07	7.90	0.64	10.60	36.90	43.00	0.68
Winter	28040	17.02	24.18	7.91	8.83	0.62	10.28	35.60	45.50	0.68
PM_{10}										
Annual	226954	29.27	22.56	22.98	16.61	0.52	21.29	-20.10	40.80	0.66
Spring	57618	28.65	24.03	18.59	13.89	0.50	17.33	-12.20	37.50	0.67
Summer	56778	21.50	16.62	11.05	7.81	0.47	11.18	-22.40	38.60	0.63
Autumn	57100	28.47	23.09	21.05	16.34	0.56	18.78	-16.80	39.80	0.71
Winter	36494	41.45	26.59	34.55	23.83	0.47	34.88	-36.60	50.80	0.62
PM_{25}										
Annual	79664	17.52	15.07	14.65	10.29	0.65	11.39	-6.40	37.80	0.76
Spring	20200	17.28	16.59	12.53	8.36	0.59	10.16	5.20	36.10	0.72
Summer	20093	11.91	10.05	6.13	4.28	0.46	5.94	-11.50	36.80	0.64
Autumn	20932	16.46	14.65	12.43	9.74	0.69	9.26	-4.00	37.50	0.81
Winter	11344	27.53	19.67	23.01	14.97	0.61	19.87	-24.60	43.30	0.70

Table 6: Annual and seasonal scores calculated using the RB EMEP stations. The scores and the associated units are identical to the ones available on Table 4.

	nb_dly_obs	OM	MM	σ_obs	σ_mod	R	RMSE	FB	FE	IA
PM10										
Annual	6579	16.72	15.91	11.03	7.56	0.56	9.29	2.90	35.40	0.70
Spring	1697	18.26	18.11	12.08	8.47	0.49	10.83	7.20	35.20	0.66
Summer	1648	14.66	13.86	7.46	6.42	0.46	7.31	-2.30	32.10	0.67
Autumn	1620	15.25	15.93	8.80	7.75	0.65	6.98	9.80	35.30	0.80
Winter	1056	20.48	15.47	14.88	7.12	0.68	12.33	-14.40	39.40	0.68
PM2.5										
Annual	4858	11.69	10.90	9.62	5.35	0.68	7.22	8.60	42.00	0.74
Spring	1242	13.27	12.71	10.48	5.74	0.62	8.28	12.30	41.60	0.70
Summer	1202	8.69	8.60	4.55	3.39	0.36	4.58	5.80	39.10	0.59
Autumn	1217	10.00	10.32	7.12	4.78	0.67	5.30	15.70	42.70	0.78
Winter	767	16.32	11.78	13.76	6.43	0.77	10.72	-11.60	45.70	0.72
SO_4^{2-}										
Annual	10596	0.73	1.07	0.62	0.67	0.50	0.72	42.40	55.30	0.65
Spring	2830	0.75	1.19	0.54	0.56	0.57	0.67	53.70	60.80	0.66
Summer	2576	0.69	0.79	0.42	0.39	0.46	0.44	20.10	42.50	0.66
Autumn	2461	0.67	1.02	0.50	0.69	0.51	0.71	45.20	56.60	0.62
Winter	1872	0.88	1.22	0.96	0.84	0.52	0.95	43.40	57.60	0.68
NO3-										
Annual	4647	0.64	0.32	1.49	0.53	0.28	1.47	-103.50	116.20	0.34
Spring	1201	0.88	0.38	2.38	0.62	0.24	2.36	-95.00	107.80	0.26
Summer	1148	0.46	0.08	1.47	0.19	0.13	1.50	-156.10	157.10	0.12
Autumn	1141	0.49	0.28	0.59	0.44	0.48	0.58	-99.40	113.30	0.63
Winter	763	0.76	0.54	0.72	0.68	0.67	0.61	-68.40	90.20	0.79
TNO3										
Annual	7327	0.60	0.37	0.62	0.40	0.56	0.56	-55.10	71.60	0.67
Spring	1907	0.68	0.43	0.65	0.42	0.67	0.54	-50.70	66.80	0.74
Summer	1844	0.46	0.23	0.62	0.21	0.16	0.66	-66.50	75.10	0.30
Autumn	1742	0.55	0.35	0.42	0.35	0.62	0.39	-56.80	72.30	0.73
Winter	1209	0.77	0.51	0.73	0.55	0.66	0.62	-49.50	73.50	0.76
NH4+										
Annual	5427	1.01	1.14	1.63	0.81	0.43	1.47	27.10	50.60	0.53
Spring	1409	1.25	1.31	2.45	0.81	0.35	2.30	31.90	51.60	0.37
Summer	1373	0.71	0.67	1.37	0.40	0.24	1.33	7.50	42.50	0.25
Autumn	1287	0.80	1.11	0.81	0.75	0.59	0.77	39.70	56.00	0.73
Winter	902	1.37	1.47	1.29	0.97	0.77	0.83	21.10	49.30	0.85

TNH4										
Annual	4036	1.49	1.55	1.29	1.06	0.60	1.07	6.00	43.70	0.76
Spring	1036	1.66	1.91	1.30	1.26	0.58	1.20	14.30	43.20	0.74
Summer	1027	1.50	1.30	1.30	0.84	0.58	1.08	-10.70	35.90	0.70
Autumn	1005	1.43	1.54	1.34	1.02	0.61	1.08	10.80	44.90	0.76
Winter	629	1.47	1.41	1.28	0.96	0.69	0.93	-1.80	48.20	0.81

604
605

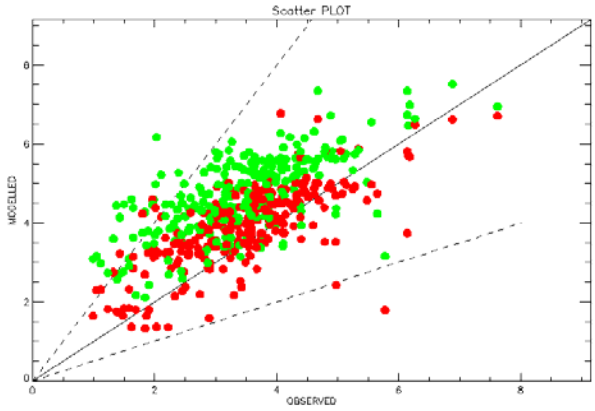

606

607 *Figure 1: Observed wind speeds (m/s) against IFS (red dots) and GFS/WRF (green dots) modelled*
608 *values for rural background stations in January 2009*

609

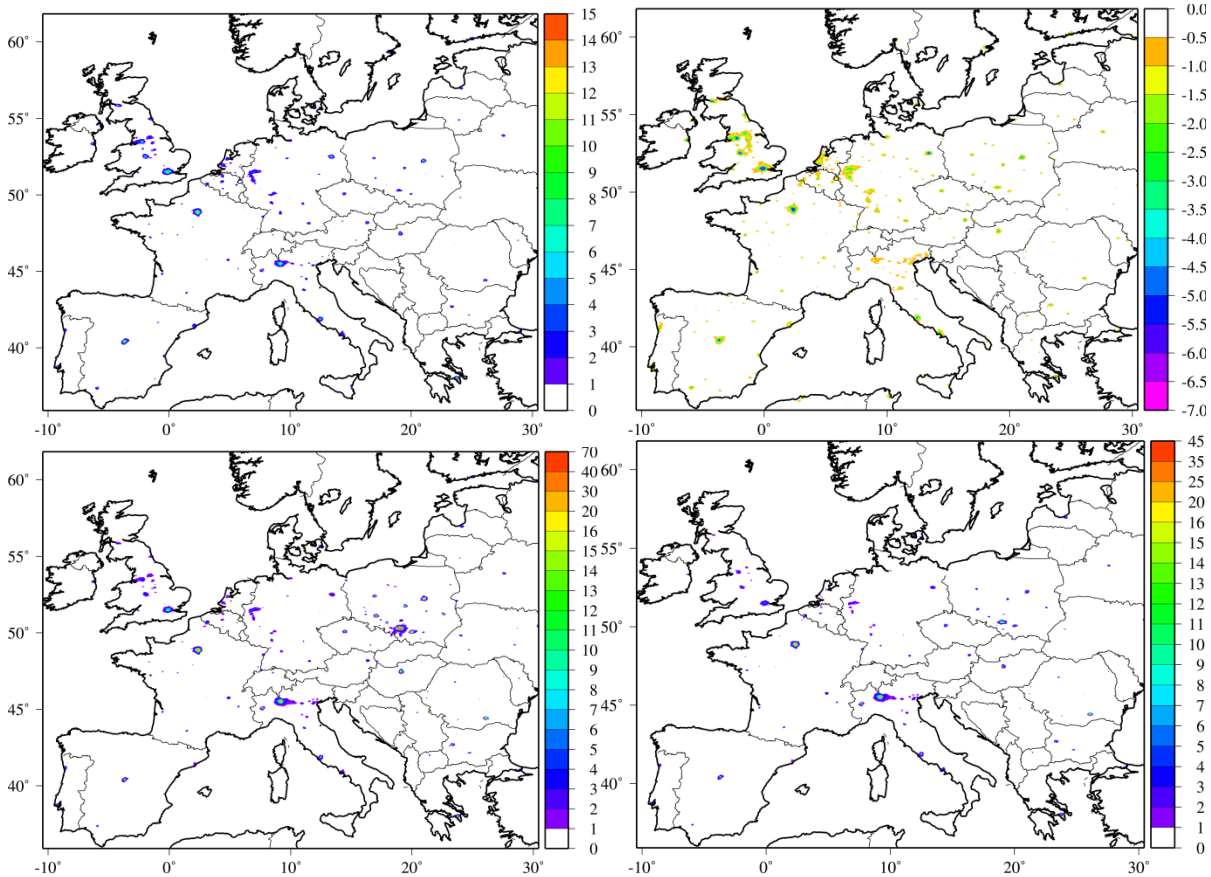

610

611

612 *Figure 2: Difference in concentrations for four main pollutants between the simulation using the*
613 *urban correction and the simulation not using the urban correction for NO_2 in ppb (top left), O_3 in ppb*
614 *(top right), PM10 in µg/m^3 (bottom left) and PM2.5 µg/m^3 (bottom right).*

615
616
617
618
619
620
621
622

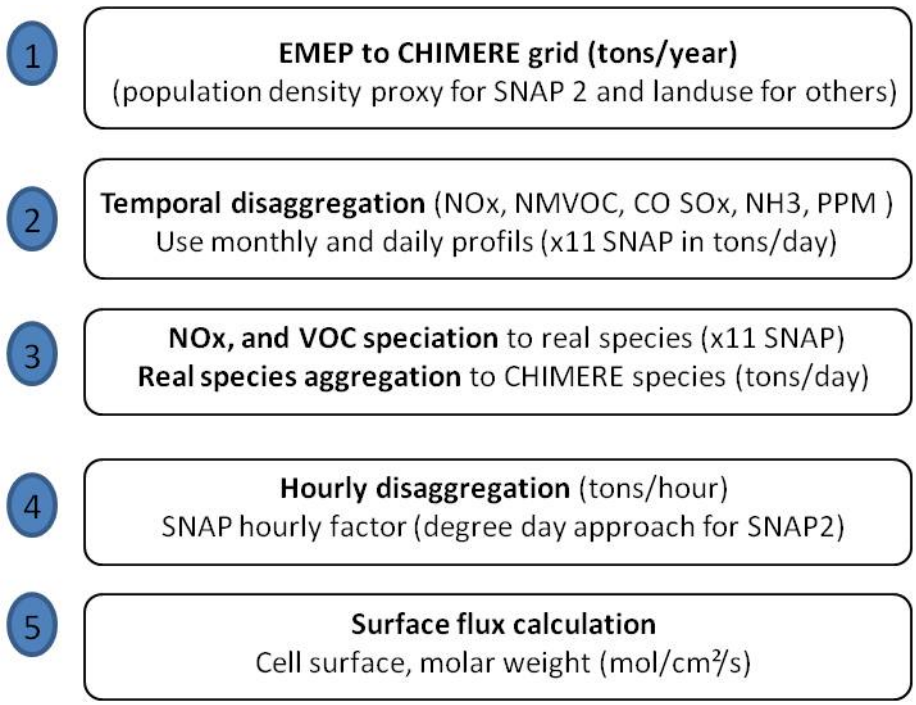

Figure 3: The EMEP to CHIMERE emission converter (adapted from Menut et al. 2012)

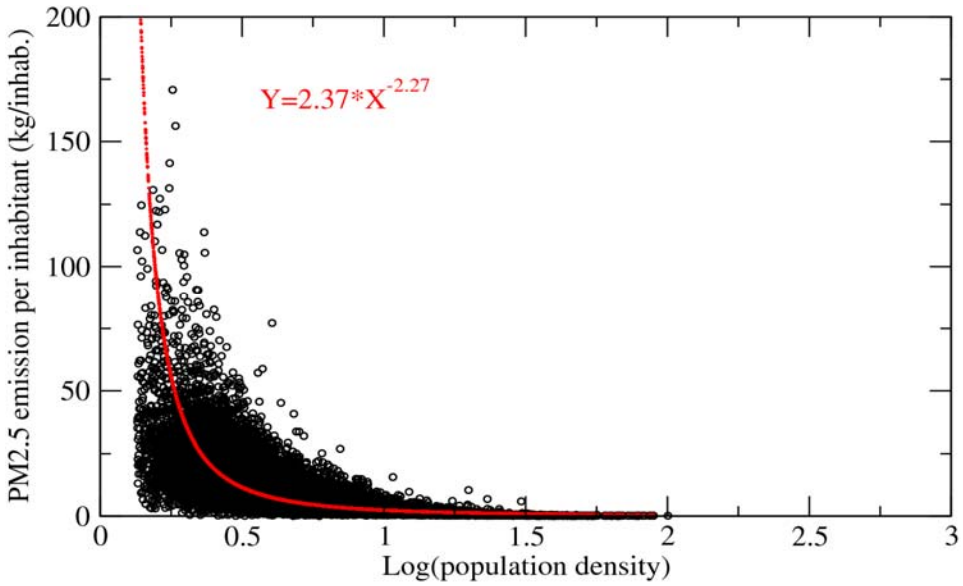

Figure 4: Evolution of PM2.5 residential emissions per inhabitant (kg/inh/year) as a function of population density (source: French National Emission Inventory). The red curve is the corresponding logarithmic regression used in the CHIMERE emission pre-processor.

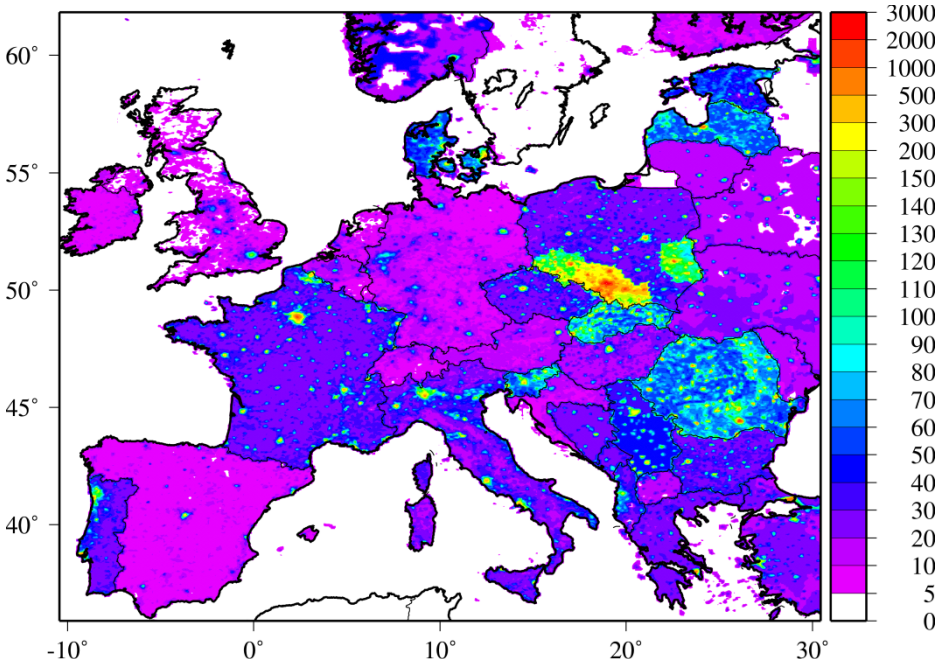

Figure 5: Total annual primary particle emission with diameter below 2.5µm from SNAP2 (g/km^2)

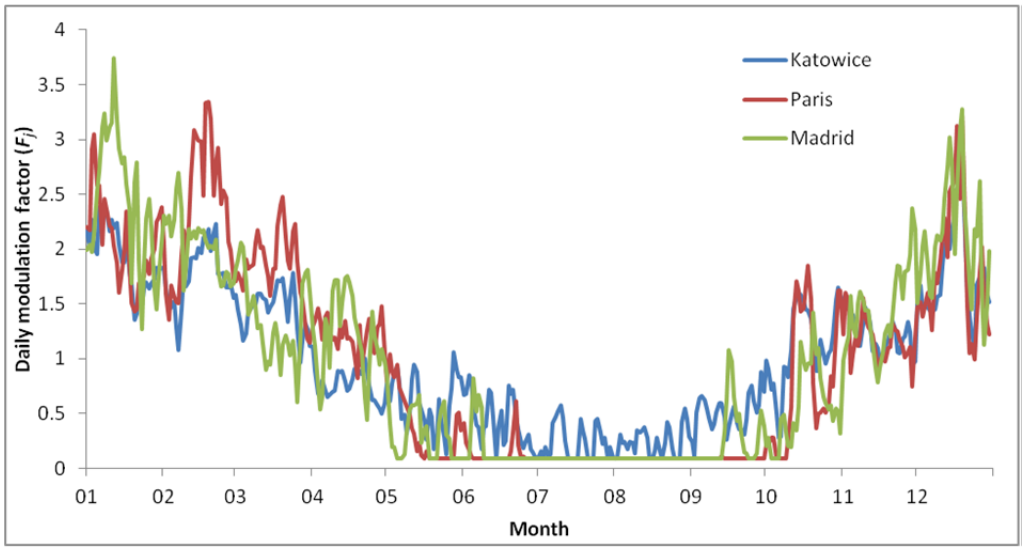

Figure 6: Daily modulation factor (Fj) apply for the SNAP 2 emission over the city of Katowice, Paris and Madrid for the year 2009

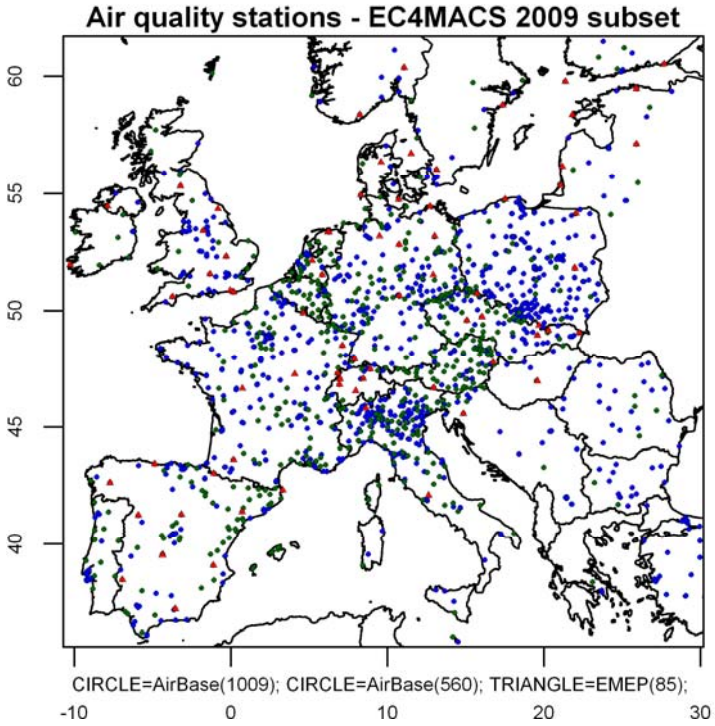

Figure 7: Airbase RB (green), Airbase UB (blue) and EMEP stations (orange) projected on the simulation domain used for the evaluation

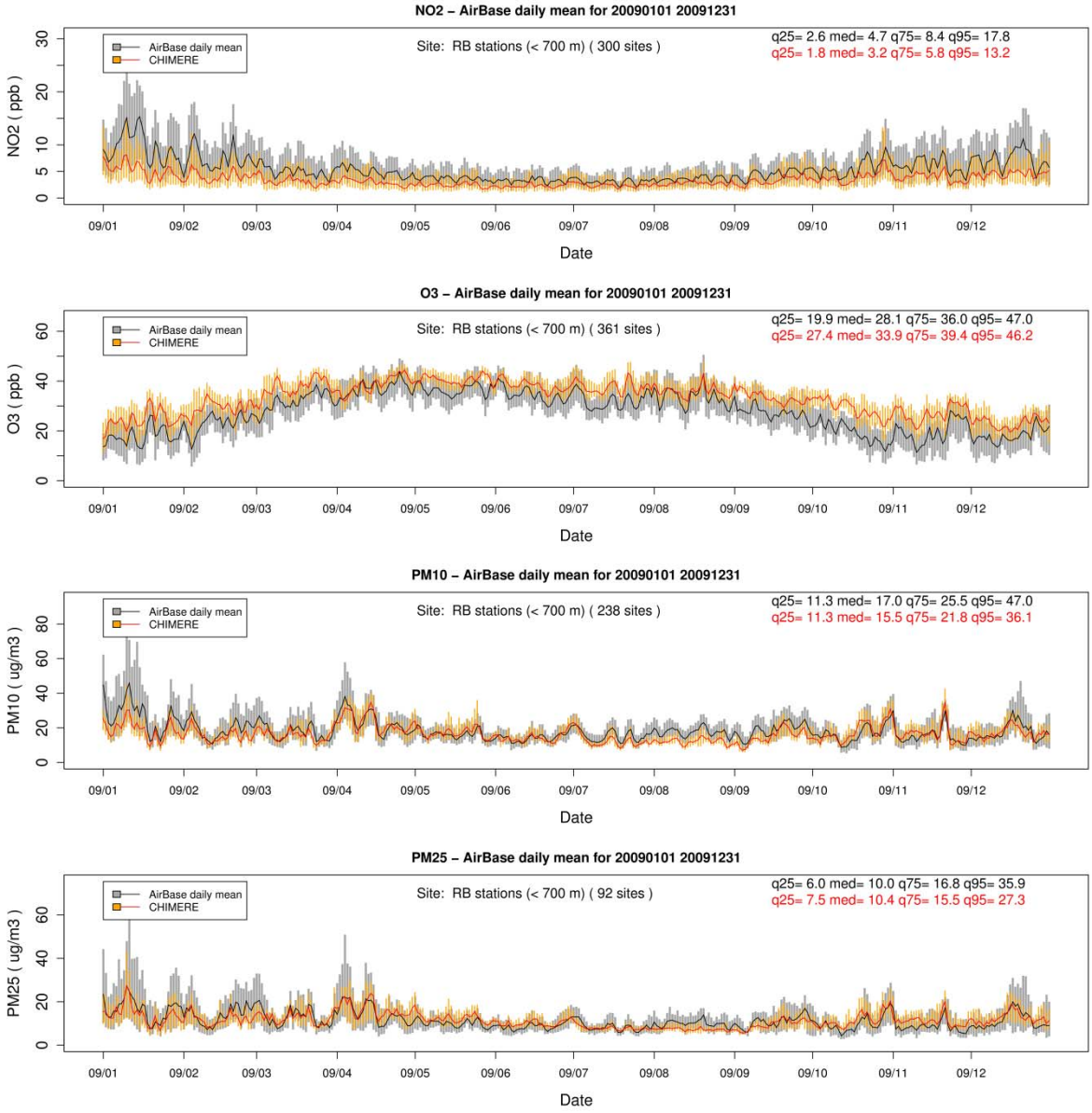

Figure 8: Daily box-whisker plots time series of the NO_2, O_3, PM_{10} and $PM_{2.5}$ observed and calculated concentrations averaged over all RB Airbase stations. The continuous lines represent the medians and the bars show the 25th -75th quantile interval. The yearly 25^{th}, 50^{th}, 75^{th}, and 95^{th} quantiles are reported on the top right corner of the plots

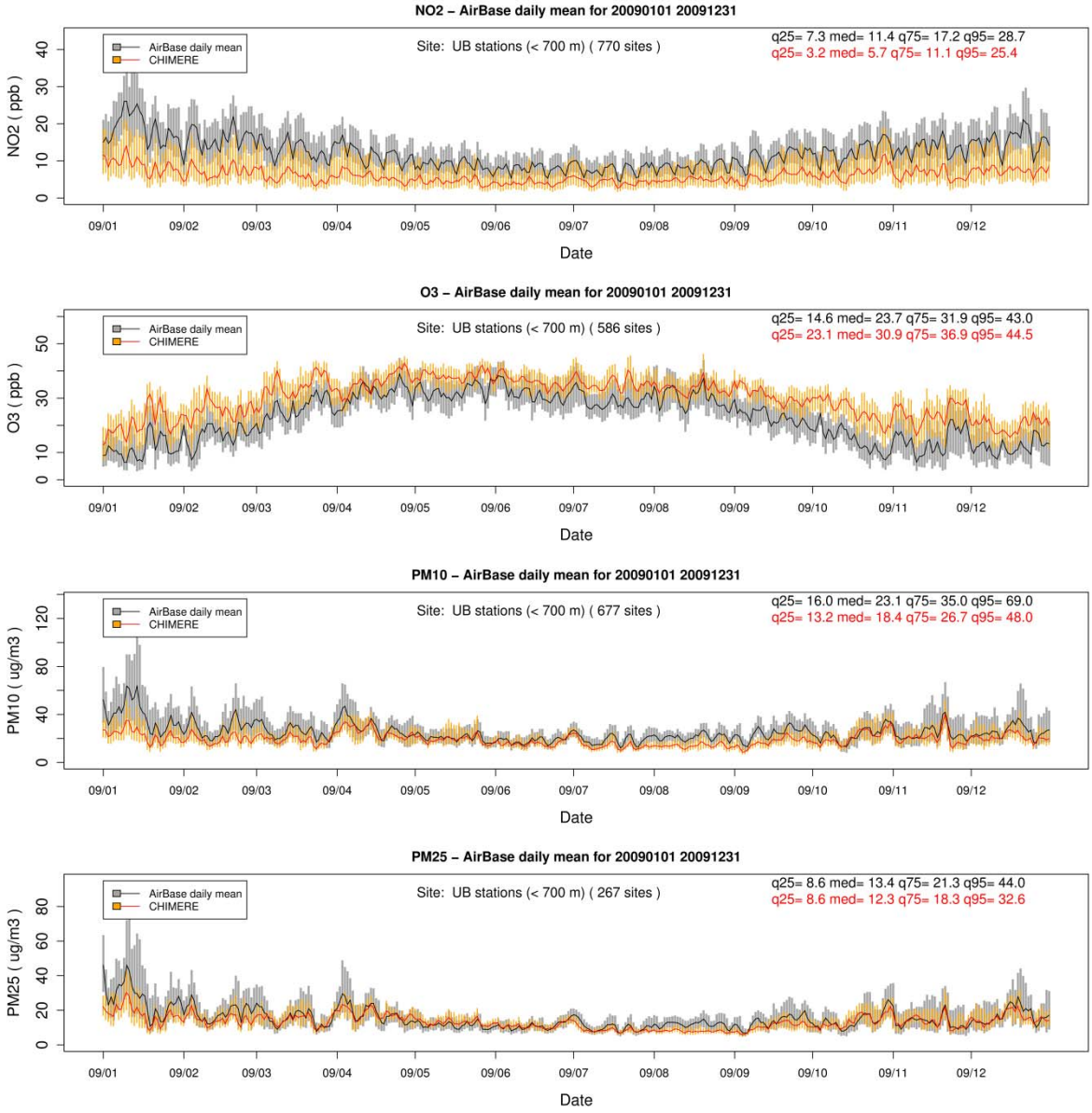

Figure 9: Same as Figure 7 but averaged over all UB Airbase stations

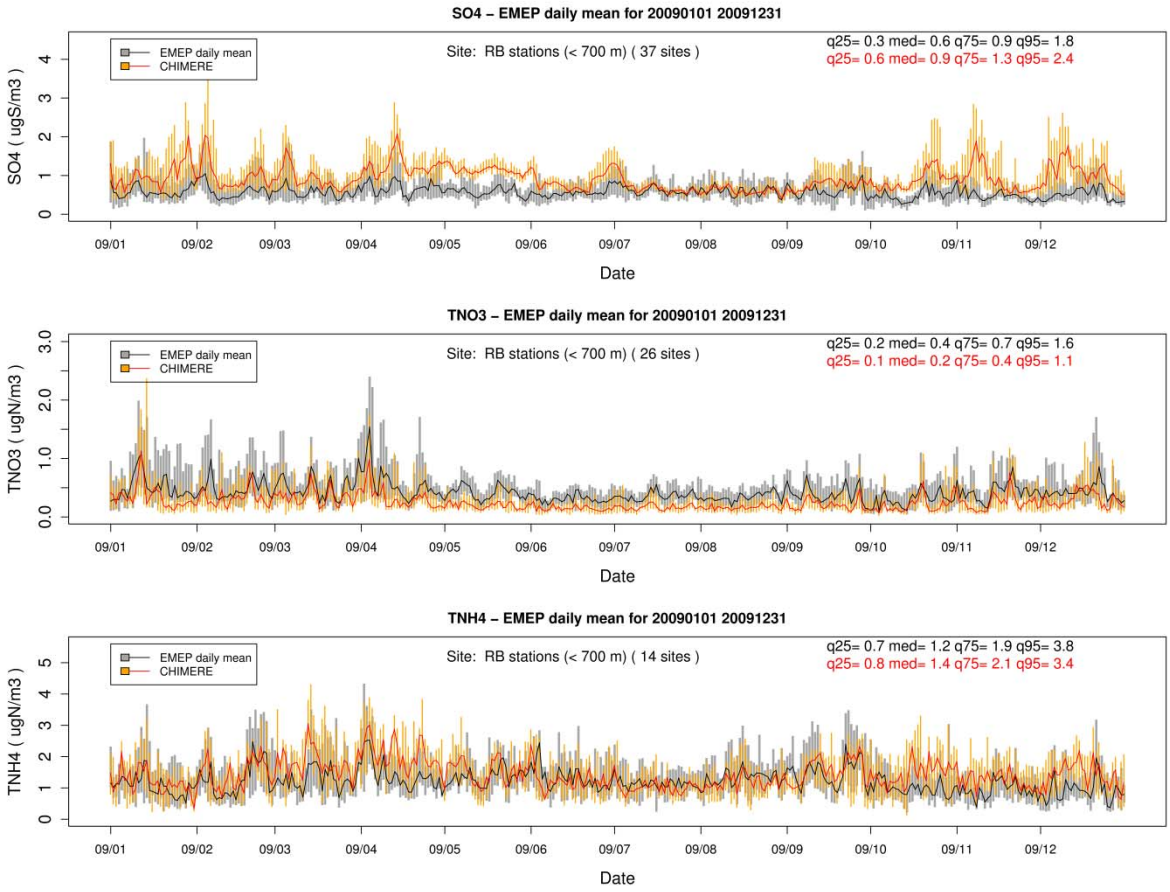

Figure 10: Same as Figure 9 but for sulphate, total nitrate (HNO_3+NO_3^-) and total ammonia (NH_3+NH_4^+) averaged over all RB EMEP stations

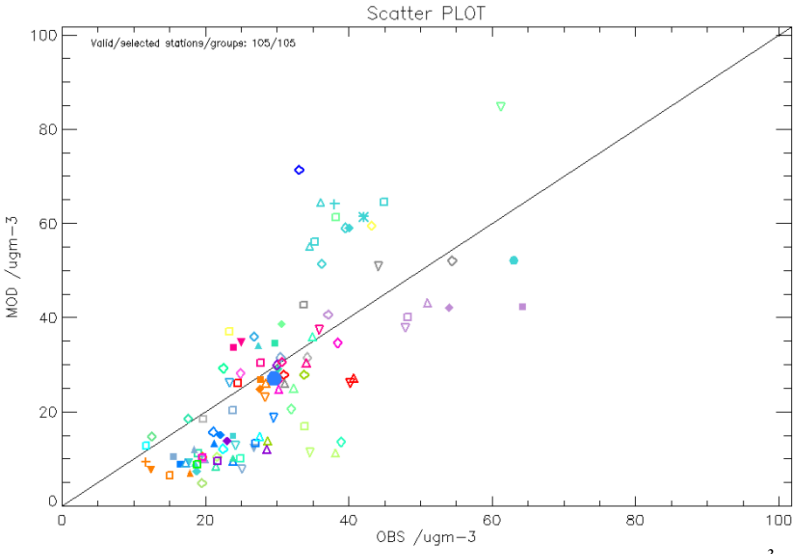

Figure 11: Scatter plot of the modelled versus observed NO_2 concentrations ($\mu g/m^3$) at the UB stations (N=105) of 30 major cities across Europe. The blue dot represents the mean of the 105 UB stations

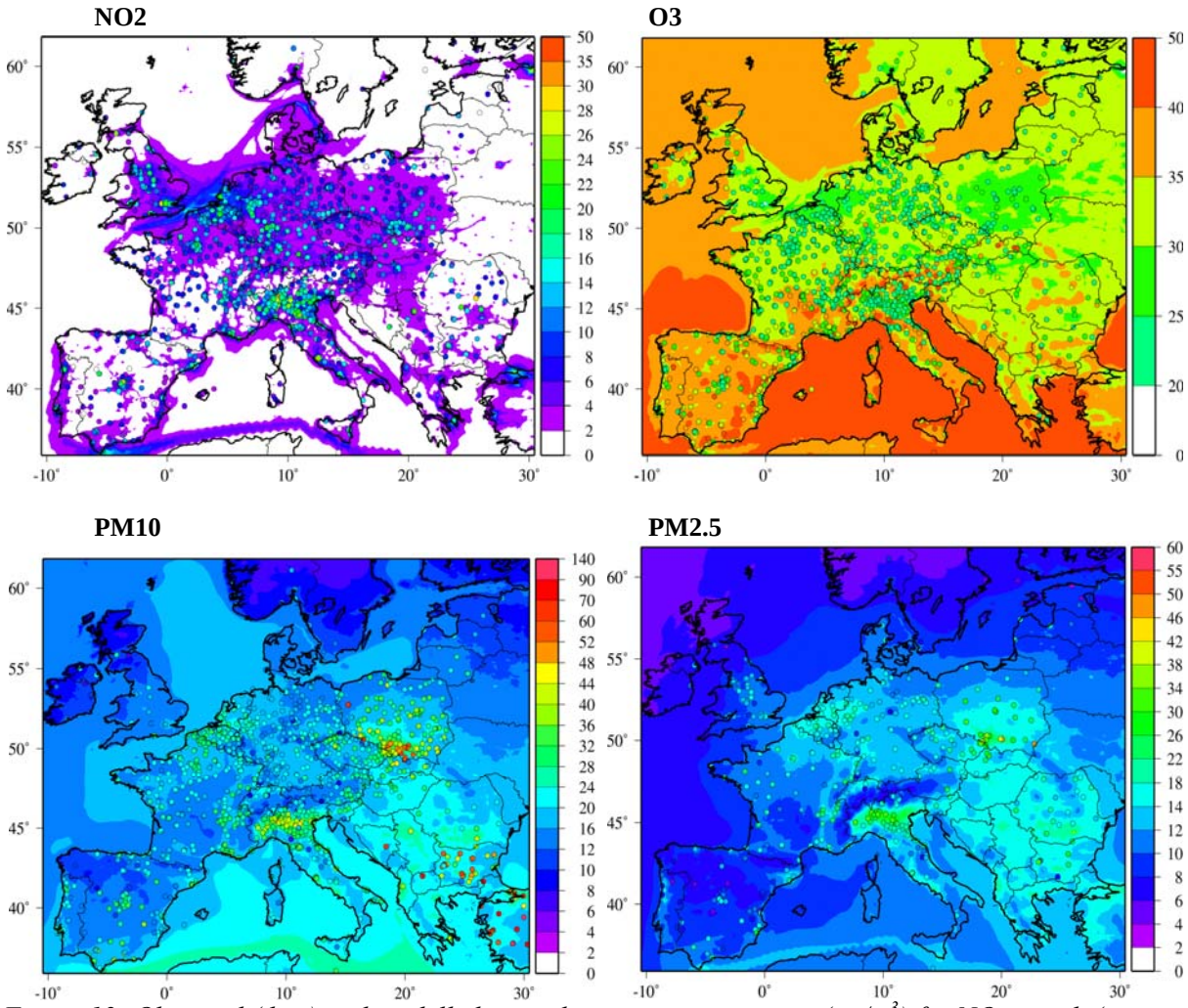

Figure 12: Observed (dots) and modelled annual mean concentrations (µg/m^3) for NO_2 in ppb (top left), O_3 in ppb (top right), PM10 (bottom left) and PM2.5 in µg/m^3 (bottom right).

NO_2

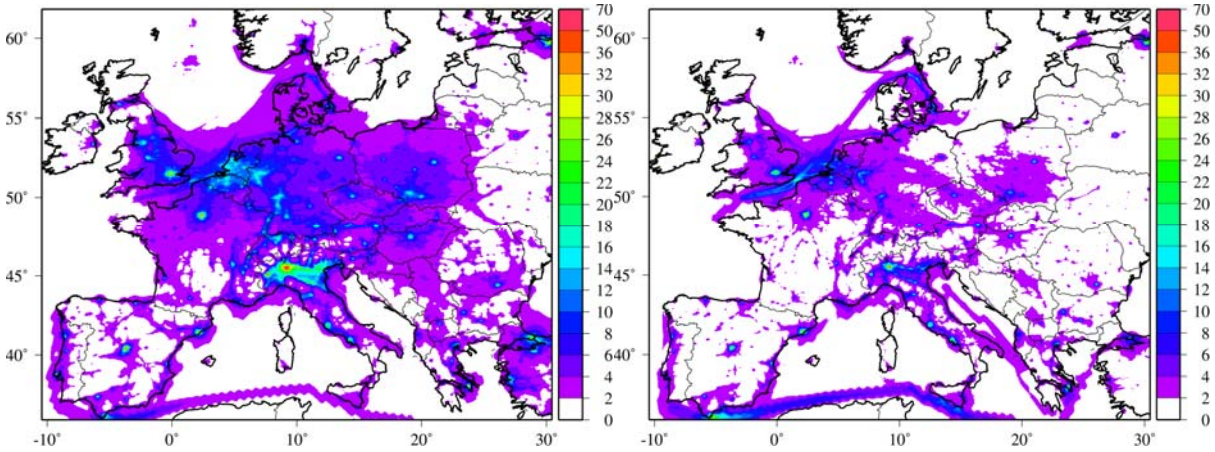

O_3

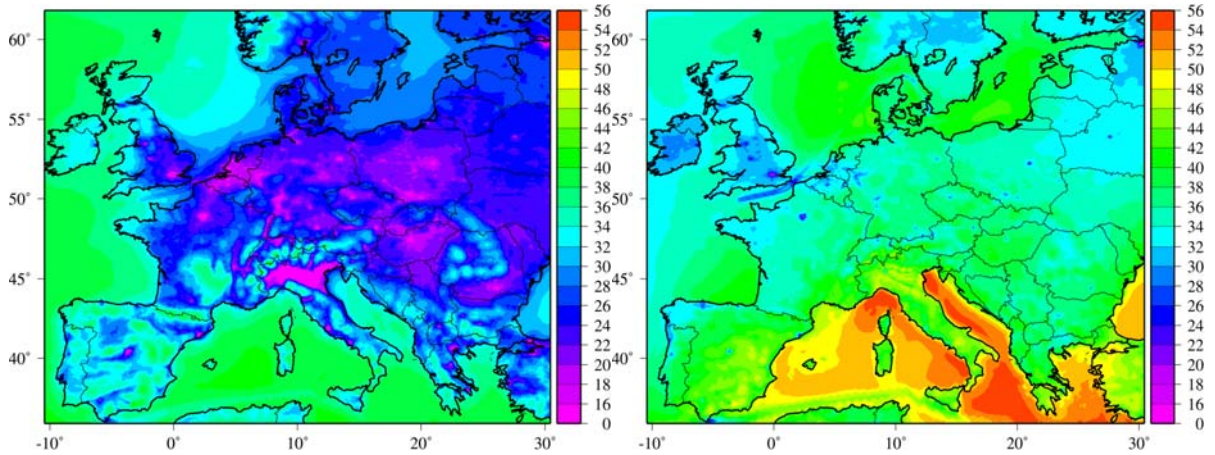

Figure 13: Modelled NO_2 and O_3 (ppb) concentrations fields calculated for the summer (left) and the winter (right).

PM_{10}

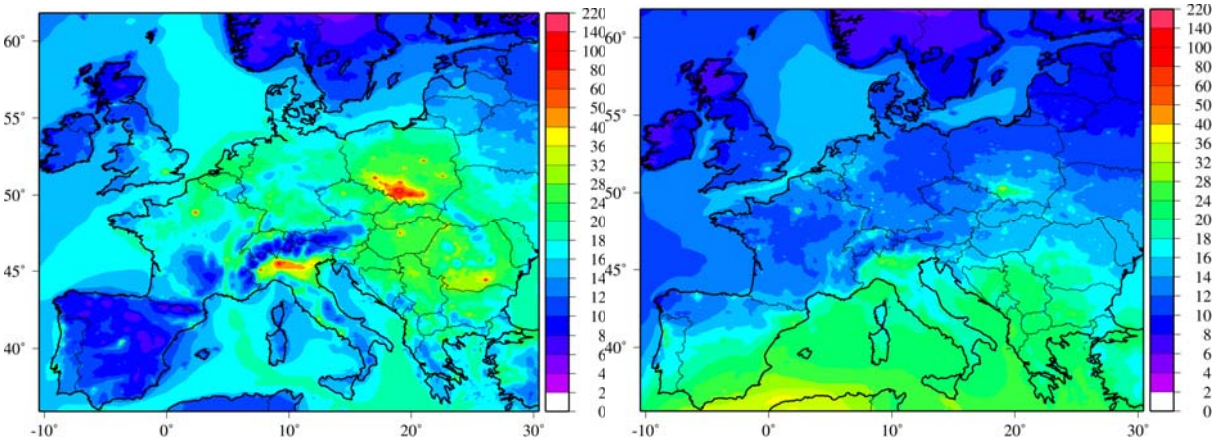

$PM_{2.5}$

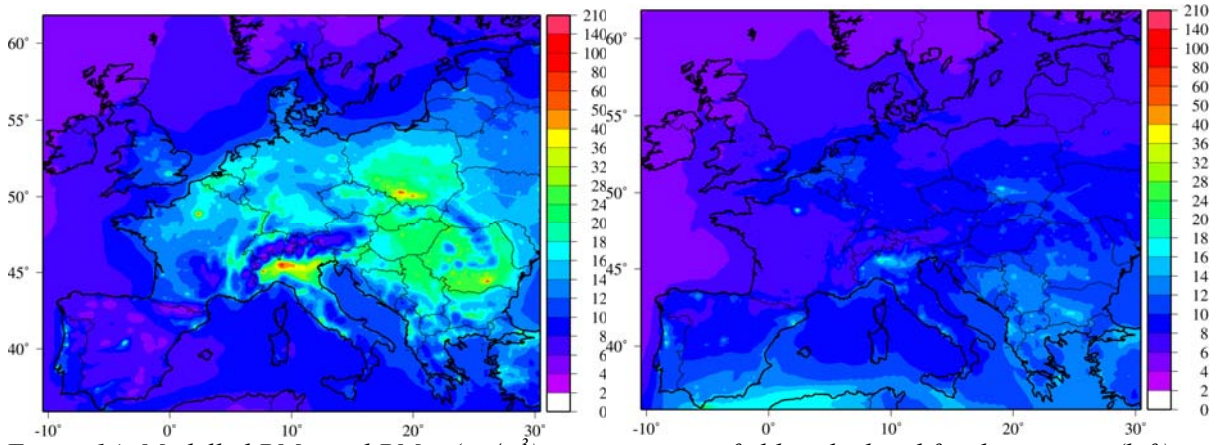

Figure 14: Modelled PM_{10} and $PM_{2.5}$ ($\mu g/m^3$) concentrations fields calculated for the summer (left) and the winter (right).

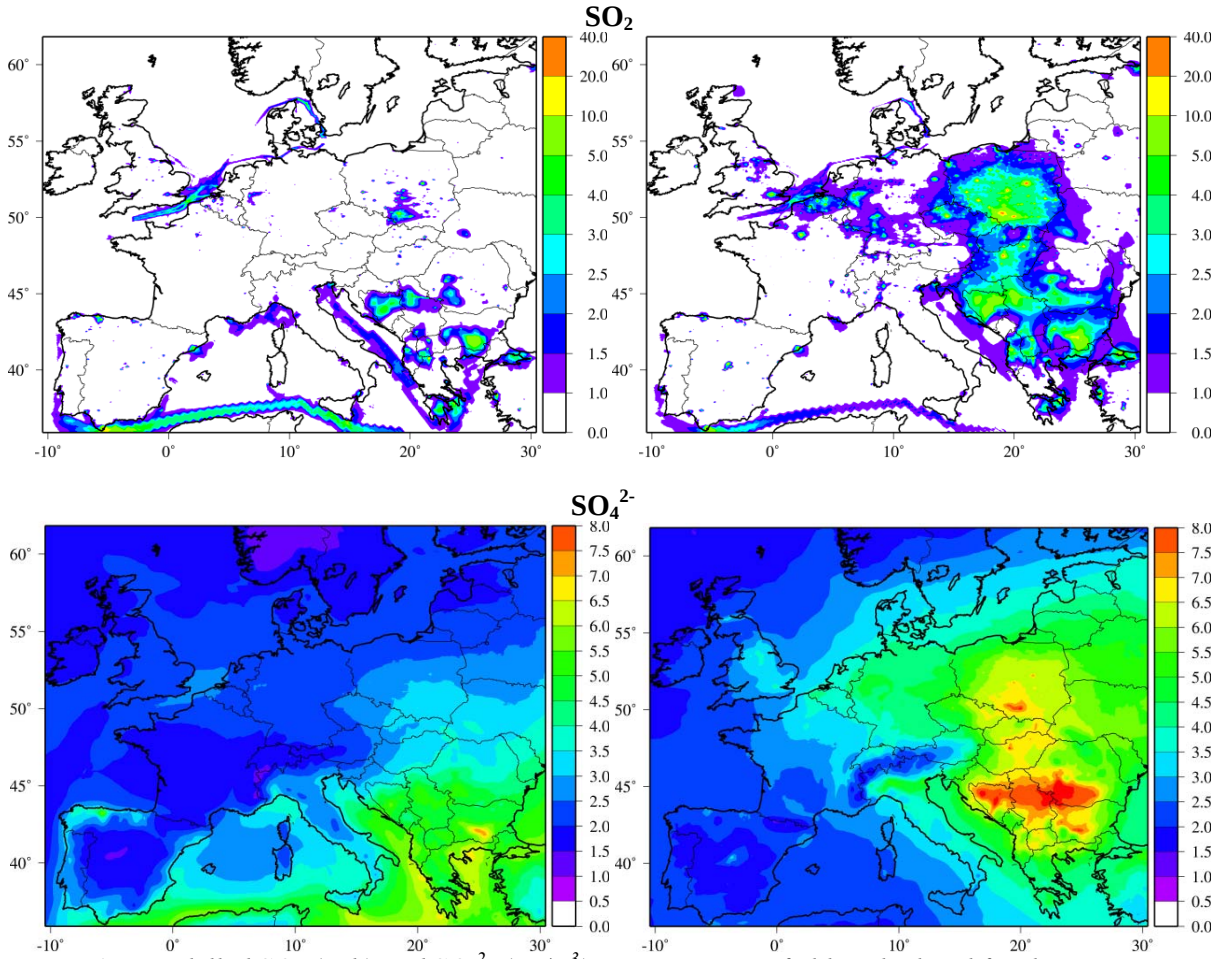

Figure 15: Modelled SO_2 (ppb) and SO_4^{2-} ($\mu g/m^3$) concentrations fields calculated for the summer (left) and the winter (right).

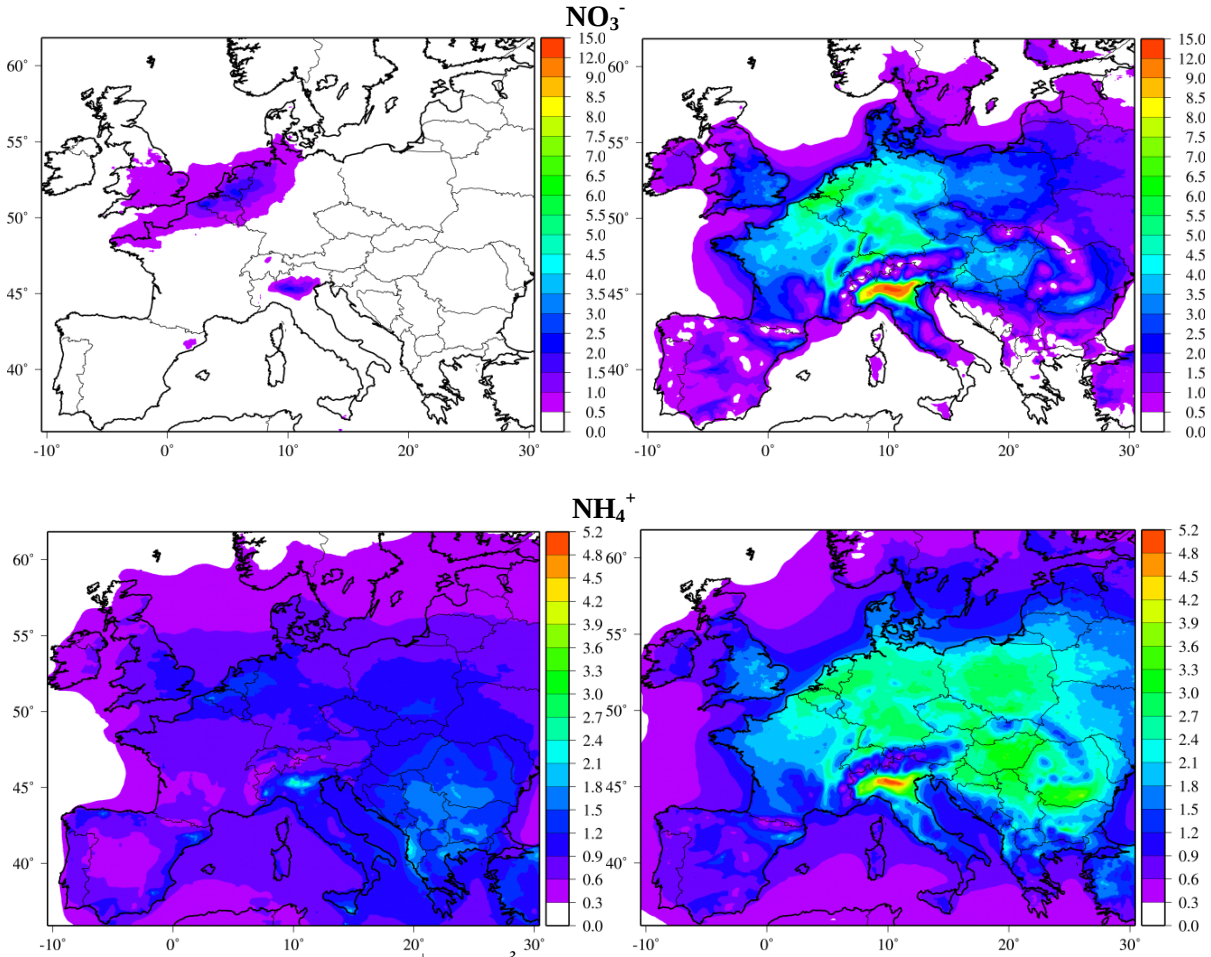

Figure 16: Modelled NO_3^- and NH_4^+ ($\mu g/m^3$) concentrations fields calculated for the summer (left) and the winter (right).

APPENDIX A

The statistical indicators selected for the operational evaluation are described below:

$$\mathrm{OM} = \frac{1}{N}\sum_{t=1}^{N} obs \tag{A1}$$

$$\mathrm{MM} = \frac{1}{N}\sum_{t=1}^{N} mod \tag{A2}$$

$$\sigma\_\mathrm{obs} = \frac{1}{N}\sum_{t=1}^{N}\sqrt{\left(\mathrm{obs(x,t)} - \overline{\mathrm{obs(x)}}\right)^2} \tag{A3}$$

$$\sigma\_\mathrm{mod} = \frac{1}{N}\sum_{t=1}^{N}\sqrt{\left(\mathrm{mod(x,t)} - \overline{\mathrm{mod(x)}}\right)^2} \tag{A4}$$

$$\mathrm{FB} = \frac{1}{N}\sum_{t=1}^{N}\frac{\mathrm{mod(x,t)} - \mathrm{obs(x,t)}}{(\mathrm{obs(x,t)} + \mathrm{mod(x,t)})/2} \tag{A5}$$

$$\mathrm{FE} = \frac{1}{N}\sum_{t=1}^{N}\frac{|\mathrm{mod(x,t)} - \mathrm{obs(x,t)}|}{(\mathrm{obs(x,t)} + \mathrm{mod(x,t)})/2} \tag{A6}$$

$$\mathrm{R} = \frac{\sum_{t=1}^{N}(\mathrm{mod(x,t)} - \overline{\mathrm{mod(x)}})\cdot(\mathrm{obs(x,t)} - \overline{\mathrm{obs(x)}})}{\sqrt{\sum_{t=1}^{N}(\mathrm{mod(x,t)} - \overline{\mathrm{mod(x)}})^2}\cdot\sqrt{\sum_{t=1}^{N}(\mathrm{obs(x,t)} - \overline{\mathrm{obs(x)}})^2}} \tag{A7}$$

$$\mathrm{IA} = 1 - \frac{\sum_{t=1}^{N}(\mathrm{mod(x,t)} - \mathrm{obs(x,t)})^2}{\sum_{t=1}^{N}(|\mathrm{mod(x,t)} - \overline{\mathrm{obs(x)}}| - |\mathrm{obs(x,t)} - \overline{\mathrm{obs(x)}}|)^2} \tag{A8}$$

$$\mathrm{RMSE} = \sqrt{\frac{1}{N}\sum_{t=1}^{N}(\mathrm{mod(x,t)} - \mathrm{obs(x,t)})^2} \tag{A9}$$

mod(*x*,*t*) – computed concentration; *obs*(*x*,*t*) – observed concentration; *N* – number of pairs.

A cut-off threshold has been applied to the observed concentrations to avoid numerical problems due to unrealistic observations. Thresholds have been defined as follows:

NO_2 = 0.5 ppb; O_3 = 5 ppb; PM_{10} = 1 μg m^{-3}; $PM_{2.5}$ = 1 μg m^{-3}.

SO_4^{2-} = 0.01 μg m^{-3}; NO_3^- = 0.01 μg m^{-3}; NH_4^+ = 0.01 μg m^{-3}.

TNO_3^- = 0.01 μg m^{-3}; TNH_4^+ = 0.01 μg m^{-3}.

BIBLIOGRAPHY

Altshuller, A.P., 1982. Atmospheric concentrations and distributions of chemical substances. In the Acidic Deposition Phenomenon and its Effects, US Environmental Protection Agency, Washington, DC.

Ansari, A.S., Pandis, S.N. (1998), Response of Inorganic PM to Precursor Concentrations, Environ. Sci. Technol., 32, 2706-2714.

Asman, W. A. H.: Modelling the atmospheric transport and deposition of ammonia and ammonium: an overview with special reference to Denmark, Atmos. Environ., 35, 1969–1983, 2001.

Appel, K. W., Gilliam, R. C., Davis, N., and Zubrow, A., 2011. Overview of the Atmospheric Model Evaluation Tool (AMET) v1.1 for evaluating meteorological and air quality models, *Environ. Modell. Softw.* 26, 4, 434-443.

Balk, K., Jaakko Kukkonen, Kostas Karatzas, Tassos Bassoukos, Victor Epitropou, A European open access chemical weather forecasting portal, Atmospheric Environment, Volume 45, Issue 3

Baker, K., Scheff, P., 2007. Photochemical model performance for PM2.5 sulphate, nitrate, ammonium, and precursor species SO2, HNO3, and NH3 at background monitor locations in the Central and Eastern United States. Atmospheric Environment 41, 6185e6195.Boylan, J.W., Russell, A.G., 2006.

Bauer, S. E., Koch, D., Unger, N., Metzger, S. M., Shindell, D. T., and Streets, D. G.: Nitrate aerosols today and in 2030: a global simulation including aerosols and tropospheric ozone, Atmos. Chem. Phys., 7, 5043-5059, doi:10.5194/acp-7-5043-2007, 2007.

Bessagnet B., C.Seigneur, L.Menut, 2010, Impact of dry deposition of semi-volatile organic compounds on secondary organic aerosols, Atmospheric Environment, 10.1016/j.atmosenv.2010.01.027

Bessagnet B., L.Menut, G.Curci, A.Hodzic, B.Guillaume, C.Liousse, S.Moukhtar, B.Pun, C.Seigneur, M.Schulz, 2009, Regional modeling of carbonaceous aerosols over Europe - Focus on Secondary Organic Aerosols, *Journal of Atmospheric Chemistry*, 61, 175-202

Bieser, J., A.Aulinger., V.Matthias., M.Quante., H.A.C. Denier van der Gon, Vertical emission profiles for Europe based on plume rise calculations, Environmental Pollution (2011), oi:10.1016/j.envpol.2011.04.030

Colette A., O.Favez, F.Meleux, L.Chiappini, M.Haeffelin, Y.Morille, L.Malherbe, A.Papin, B.Bessagnet, L.Menut, E.Leoz, L.Rouil, 2011, Assessing in near real time the impact of the April 2010 Eyjafjallajokull ash plume on air quality, Atmospheric Environment, 45, 1217-1221.

Coll, I., Lasry, F., Fayet, S., Armengaud, A., and R. Vautard, 2009, Simulation and evaluation of 2010 emission control scenarios in a Mediterranean area. Atmos. Environ., 43, 4194-4204.

Chen, K. S., Ho, Y. T., Lai, C. H., and Chou, Y.-M.: Photochemical modeling and analysis of meteorological parameters during ozone episodes in Kaohsiung, Taiwan, Atmos. Environ., 37(13), 18111823, 2003.

EEA (2012) Air quality in Europe — 2012 report, EEA Report No 4/2012, Office for Official Publications of the European Union, ISBN 978-92-9213-328-3.

967 Fisher, P., Kukkonen, J., Piringer, M., Rotach, M. W., and Schatzmann, M.: Meteorology applied to
968 urban air pollution problems: concepts from COST 715, *Atmos. Chem. Phys. Discuss*., 5,
969 7903-7927, doi:10.5194/acpd-5-7903-2005, 2005.

970 Hamaoui-Laguel, L., Meleux, F., Beekmann, M., Bessagnet, B., Génermont, S., Cellier, P., Létinois,
971 L., Improving ammonia emissions in air quality modelling for France, *Atmospheric*
972 *Environment* (2012), doi: 10.1016/j.atmosenv.2012.08.002.
973
974 Hodzic A, Jimenez JL, Madronich S, et al., 2010, Modeling organic aerosols in a megacity: potential
975 contribution of semi-volatile and intermediate volatility primary organic compounds to
976 secondary organic aerosol formation, Atmospheric chemistry and physics Volume: 10 Issue:
977 12 Pages: 5491-5514
978
979 Hodzic A, Bessagnet B, Vautard R, A model evaluation of coarse-mode nitrate heterogeneous
980 formation on dust particle, ATMOSPHERIC ENVIRONMENT 40 (22): 4158-4171 JUL 2006
981
982 Jimenez, P.A. and Dudhia, J, 2012. Improving the representation of resolved and unresolved
983 topographic effects on surface wind in the WRF model. J. Appl. Meteor. Climatol., 51, 300–
984 316.
985
986 Jiménez-Guerrero, P., O. Jorba, M.T. Pay, J.P. Montavez, S. Jerez, J.J. Gomez-Navarro, J.M.
987 Baldasano, 2011. Comparison of two different sea-salt aerosol schemes as implemented in air
988 quality models applied to the Mediterranean. Atmos. Chem. Phys. 11, 4833-4850, doi:
989 10.5194/acp-11-4833-2011.
990
991 Jimenez, P., Rene Parra, Jose M. Baldasano, Influence of initial and boundary conditions for ozone
992 modeling in very complex terrains: A case study in the northeastern Iberian Peninsula,
993 Environmental Modelling & Software (2006), doi:10.1016/j.envsoft.2006.08.004
994
995 Kaneyasu et al., 1995 N. Kaneyasu, S. Ohta, N. Murao. Seasonal variation in the chemical
996 composition of atmospheric aerosols and gaseous species in Sapporo, Japan, Atmos.
997 Environ., 29 (13) (1995), pp. 1559–1568
998
999 Matthias, V., 2008. The aerosol distribution in Europe derived with the Community Multiscale Air
1000 Quality (CMAQ) model: comparison to near surface in situ and sunphotometer measurements.
1001 Atmos. Chem. Phys., 8, 5077-5097.
1002
1003 Matthias, V., Armin Aulinger, Johannes Bieser, Juan Cuesta, Beate Geyer, Bärbel Langmann, Ilya
1004 Serikov, Ina Mattis, Andreas Minikin, Lucia Mona, Markus Quante, Ulrich Schumann,
1005 Bernadett Weinzierl, The ash dispersion over Europe during the Eyjafjallajökull eruption –
1006 Comparison of MAQ simulations to remote sensing and air-borne in-situ observations,
1007 Atmospheric Environment, volume 48, March 2012, Pages 184-194, ISSN 1352-2310,
1008 1016/j.atmosenv.2011.06.077.
1009
1010 Mass, C.F. and Ovens, D. (2011) 'Fixing WRF's high speed wind bias: a new subgrid scale drag
1011 parameterization and the role of detailed verification'. 91st *AMS Annual Meeting*, Seattle, WA.
1012 Available at http://ams.confex.com/ams/91Annual/webprogram/Paper180011.html (accessed
1013 3 November 2011).
1014
1015 Menut, L. and Bessagnet, B.: Atmospheric composition forecasting in Europe, Ann. Geophys., 28, 61–
1016 74, doi:10.5194/angeo-28-61- 2010, 2010.
1017
1018 Pay, M.T., Jiménez-Guerrero, P., Jorba, O., Basart, S., Querol, X., Pandolfi, M., Baldasano, J.M.
1019 Spatio-temporal variability of concentrations and speciation of particulate matter across spain

in the caliope modeling system, Atmospheric Environment (2011), doi: 10.1016/, j.atmosenv.2011.09.049

Kukkonen, J., Balk, T., Schultz, D. M., Baklanov, A., Klein, T., Miranda, A. I., Monteiro, A., Hirtl, M., Tarvainen, V., Boy, M., Peuch, V.-H., Poupkou, A., Kioutsioukis, I., Finardi, S., Sofiev, M., Sokhi, R., Lehtinen, K., Karatzas, K., San José, R., Astitha, M., Kallos, G., Schaap, M., Reimer, E., Jakobs, H., and Eben, K.: Operational, regional-scale, chemical weather forecasting models in Europe, Atmos. Chem. Phys. Discuss., 11, 5985-6162, doi:10.5194/acpd-11-5985-2011.

Richards, L.W., 1983. Comments on the oxidation of NO2 to nitrate: day and night. Atmos. Environ. 17, 397–402

Russell, A.G., Cass, G.R., Seinfeld, J.H., 1986. On some aspects of nighttime atmospheric chemistry. Environ. Sci. Technol. 20, 1167–1172.

Sarrat C., Lemonsu A., Masson V. et Guedalia D. (2006). Impact of urban heat island on regional atmospheric pollution. *Atmospheric Environment* 40(10): 1743-1758.

Siedlecki, M, Urban – rural wind speed differences in Lodz, University of Lodz, Poland. Online resource.

Solazzo, E., Di Sabatino, S., Aquilina, N., Dudek, A., Britter, R., Coupling Mesoscale Modelling with a Simple Urban Model: The Lisbon Case Study, *Boundary-Layer Meteorol* 137:441–457, DOI 10.1007/s10546-010-9536-6, 2010.

Szopa, S., Foret, G., Menut, L., and Cozic, A.: Impact of large scale circulation on European summer surface ozone and consequences for modelling forecast, Atmos. Environ., 43, 1189–1195, 2009.

Thunis P., E. Georgieva, A. Pederzoli, A tool to evaluate air quality model performances in regulatory applications, Environmental Modelling and Software, Volume 38, December 2012, Pages 220-230, ISSN 1364-8152, 10.1016/j.envsoft.2012.06.005.

Vautard R., M.Maidi, L.Menut, M.Beekmann, A.Colette, 2007, Boundary layer photochemistry simulated with a two-stream convection scheme,, *Atmospheric Environment*, Volume 41, Issue 37, pp.8275-8287.

Vautard R., B.Bessagnet, M.Chin and L. Menut, 2005, On the contribution of natural Aeolian sources to particulate matter concentrations in Europe: testing hypotheses with a modelling approach, *Atmospheric Environment*, 39, Issue 18, 3291-3303